THE UNIVERSITY of EDINBURGH

Edinburgh Research Explorer

Heparan sulphate sulphation by Hs2st restricts astroglial precursor somal translocation in developing mouse forebrain by a non cell autonomous mechanism

Citation for published version:
Clegg, J, Parkin, H, Mason, J & Pratt, T 2019, 'Heparan sulphate sulphation by Hs2st restricts astroglial precursor somal translocation in developing mouse forebrain by a non cell autonomous mechanism', *Journal of Neuroscience*. https://doi.org/10.1523/JNEUROSCI.1747-17.2018

Digital Object Identifier (DOI):
10.1523/JNEUROSCI.1747-17.2018

Link:
Link to publication record in Edinburgh Research Explorer

Document Version:
Peer reviewed version

Published In:
Journal of Neuroscience

General rights
Copyright for the publications made accessible via the Edinburgh Research Explorer is retained by the author(s) and / or other copyright owners and it is a condition of accessing these publications that users recognise and abide by the legal requirements associated with these rights.

Take down policy
The University of Edinburgh has made every reasonable effort to ensure that Edinburgh Research Explorer content complies with UK legislation. If you believe that the public display of this file breaches copyright please contact openaccess@ed.ac.uk providing details, and we will remove access to the work immediately and investigate your claim.

Download date: 11. May. 2020

This Accepted Manuscript has not been copyedited and formatted. The final version may differ from this version.

JNeurosci
THE JOURNAL OF NEUROSCIENCE

JNeurosci Accepted Manuscript

Research Articles: Development/Plasticity/Repair

Heparan sulphate sulphation by Hs2st restricts astroglial precursor somal translocation in developing mouse forebrain by a non cell autonomous mechanism

James M. Clegg[1,2], Hannah Parkin[2], John O. Mason[1,2] and Thomas Pratt[1,2]

[1]*Simons Initiative for the Developing Brain*

[2]*Centre for Discovery Brain Sciences,, Hugh Robson Building, Edinburgh Medical School Biomedical Sciences, The University of Edinburgh, Edinburgh, United Kingdom, EH8 9XD, United Kingdom.*

https://doi.org/10.1523/JNEUROSCI.1747-17.2018

Received: 22 June 2017

Revised: 5 December 2018

Accepted: 11 December 2018

Published: 7 January 2019

Author contributions: J.M.C., H.M.P., J.O.M., and T.P. designed research; J.M.C. and H.M.P. performed research; J.M.C. and H.M.P. analyzed data; J.M.C., H.M.P., and T.P. wrote the paper.

Conflict of Interest: The authors declare no competing financial interests.

We are grateful to the following people for supplying us with transgenic mouse lines: ***Hs2stfl***, Jeffrey Esko (University College San Diego); ***Ext1fl***, Yu Yamaguchi (Sanford Burnham Institute); ***Zic4Cre*** and ***Emx1CreER***, Nicoletta Kessaris (University College London). We would like to thank the anonymous reviewers whose comments have helped us improve the manuscript from its initial submission. This work was supported by grants from The Wellcome Trust (094832/Z/10/Z) and BBSRC (BB/M00693X/1) to TP and an EASTBIO BBSRC funded PhD studentship to HP.

Correspondence should be addressed to Senior Author and correspondence: t.pratt@ed.ac.uk

Cite as: J. Neurosci 2019; 10.1523/JNEUROSCI.1747-17.2018

Alerts: Sign up at www.jneurosci.org/alerts to receive customized email alerts when the fully formatted version of this article is published.

Accepted manuscripts are peer-reviewed but have not been through the copyediting, formatting, or proofreading process.

Copyright © 2019 Clegg et al.
This is an open-access article distributed under the terms of the Creative Commons Attribution 4.0 International license, which permits unrestricted use, distribution and reproduction in any medium provided that the original work is properly attributed.

JNeurosci Accepted Manuscript

1 **Title Page.**

2 **Title: Heparan sulphate sulphation by Hs2st restricts astroglial precursor somal**
3 **translocation in developing mouse forebrain by a non cell autonomous mechanism.**

4 **Abbreviated title:** Hs2st and FGF signalling in developing mouse brain.

5 **James M. Clegg[1,2,3], Hannah Parkin[2,3], John O. Mason[1,2], and Thomas Pratt[1,2,4]**
6 [1]Simons Initiative for the Developing Brain,
7 [2]Centre for Discovery Brain Sciences,
8 Hugh Robson Building, Edinburgh Medical School Biomedical Sciences, The University
9 of Edinburgh, Edinburgh, United Kingdom, EH8 9XD, United Kingdom.
10 [3]These authors contributed equally to this work
11 [4]Senior Author and correspondence: t.pratt@ed.ac.uk

12 **Number of Pages (excluding figures):** 34
13 **Number of figures:** 11
14
15 **Number of words:**
16 **Abstract:** 250
17 **Introduction:** 780
18 **Discussion:** 2122
19
20 **Conflict of interest:** The authors declare no competing financial interests
21
22 **Acknowledgements:** We are grateful to the following people for supplying us with
23 transgenic mouse lines: *Hs2st*^{fl}, Jeffrey Esko (University College San Diego); *Ext1*^{fl}, Yu
24 Yamaguchi (Sanford Burnham Institute); *Zic4*^{Cre} and *Emx1*^{CreER}, Nicoletta Kessaris
25 (University College London). We would like to thank the anonymous reviewers whose
26 comments have helped us improve the manuscript from its initial submission. This work was
27 supported by grants from The Wellcome Trust (094832/Z/10/Z) and BBSRC
28 (BB/M00693X/1) to TP and an EASTBIO BBSRC funded PhD studentship to HP.
29
30 **Abstract**
31 Heparan sulphate (HS) is a cell surface and extracellular matrix carbohydrate extensively
32 modified by differential sulphation. HS interacts physically with canonical fibroblast growth
33 factor (FGF) proteins that signal through the extracellular signal regulated kinase

JNeurosci Accepted Manuscript

34 (ERK)/mitogen activated kinase (MAPK) pathway. At the embryonic mouse telencephalic
35 midline FGF/ERK signalling drives astroglial precursor somal translocation from the
36 ventricular zone of the cortico-septal boundary (CSB) to the induseum griseum (IG)
37 producing a focus of *Slit2*-expressing astroglial guidepost cells essential for inter-hemispheric
38 corpus callosum (CC) axon navigation. Here we investigate the cell and molecular function
39 of a specific form of HS sulphation, 2-O HS sulphation catalysed by the enzyme Hs2st, in
40 midline astroglial development and in regulating FGF protein levels and interaction with HS.
41 *Hs2st*$^{-/-}$ embryos of either sex exhibit a grossly enlarged IG due to precocious astroglial
42 translocation and conditional *Hs2st* mutagenesis and *ex vivo* culture experiments show that
43 *Hs2st* is not required cell autonomously by CC axons or by the IG astroglial cell lineage but
44 rather acts non cell autonomously to suppress the transmission of translocation signals to
45 astroglial precursors. Rescue of the *Hs2st*$^{-/-}$ astroglial translocation phenotype by
46 pharmacologically inhibiting FGF signalling shows the normal role of Hs2st is to suppress
47 FGF-mediated astroglial translocation. We demonstrate a selective action of Hs2st on FGF
48 protein by showing that *Hs2st* (but not *Hs6st1*) normally suppresses the levels of Fgf17
49 protein in the CSB region *in vivo* and use a biochemical assay to show *Hs2st* (but not *Hs6st1*)
50 facilitates physical interaction between Fgf17 protein and HS.
51
52 **Significance statement.**
53 We report a novel non cell autonomous mechanism regulating cell signalling in developing
54 brain. Using the developing mouse telencephalic midline as an exemplar we show that the
55 specific sulphation modification of the cell surface and extracellular carbohydrate heparan
56 sulphate (HS) performed by Hs2st suppresses the supply of translocation signals to astroglial
57 precursors by a non cell autonomous mechanism. We further show that Hs2st modification
58 selectively facilitates physical interaction between Fgf17 and HS and supresses Fgf17 protein
59 levels *in vivo*, strongly suggesting that Hs2st acts selectively on Fgf17 signalling. HS
60 interacts with many signalling proteins potentially encoding numerous selective interactions
61 important in development and disease so this class of mechanism may apply more broadly to
62 other biological systems.
63
64 **Introduction**
65 The corpus callosum (CC) axon tract connects the cerebral hemispheres through the
66 cortico-septal boundary (CSB) in mice and humans and CC malformation is associated with
67 cognitive and neurological conditions in humans (Donahoo and Richards, 2009). Precisely

JNeurosci Accepted Manuscript

68 controlled radial glial cell (RGC) somal translocation from the ventricular zone (VZ) of the
69 CSB to its pial surface generates midline zipper (MZ) and induium griseum (IG) astroglial
70 populations required for cerebral hemisphere fusion and subsequent CC axon navigation
71 (Clegg et al., 2014; Gobius et al., 2016; Inatani et al., 2003; Moldrich et al., 2010; Shu and
72 Richards, 2001; Shu et al., 2003; Smith et al., 2006). The movement of RGC astroglial
73 precursors from the glial wedge (GW) to the IG (GW→IG translocation) forms an astroglial
74 guidepost population that secretes Slit2 to guide CC axons across the telencephalic midline.

75 Fibroblast growth factors (FGFs) are an evolutionarily ancient family comprising 23
76 genes in mice and humans of which 15 (*Fgf1-10*,*16-18*,*20*,*22* in mice) encode 'canonical'
77 FGFs that function as paracrine signalling molecules and bind promiscuously to cell surface
78 FGF receptors (FGFRs encoded by *Fgfr1-4* in mice) to elicit an extracellular signal regulated
79 kinase (ERK)/mitogen activated kinase (MAPK) response via activating phosphorylation of
80 ERK→phospo-ERK (pERK). Canonical FGFs are further subdivided into five subfamilies
81 based on phylogeny and '*Fgf8*' subfamily members *Fgf8* and *Fgf17* are transcribed in the
82 developing CSB in close spatiotemporal proximity posing the question of how they are
83 coordinated (Guillemot and Zimmer, 2011; Ornitz and Itoh, 2015). Under normal conditions
84 GW→IG translocation is primarily attributed to Fgf8 and needs to be tightly regulated to
85 ensure correct numbers of RGCs leave the GW and reach the IG. Deviation above (or below)
86 normal FGF/ERK signalling levels induces too many (or too few) RGCs to translocate with
87 consequent disruption to CC development (Clegg et al., 2014; Gobius et al., 2016; Smith et
88 al., 2006; Wang et al., 2012). While Fgf17 plays a role in patterning the developing
89 telencephalon its importance for CC development is less clear and no CC phenotype has been
90 reported in *Fgf17*$^{-/-}$ embryos (Cholfin and Rubenstein, 2007, 2008). Because *Fgf8* and *Fgf17*
91 are the principal *Fgf's* transcribed in vicinity of the GW and both activate ERK, mechanisms
92 must exist to keep the total amount of Fgf protein (Fgf8 protein + Fgf17 protein) at the
93 correct level to generate the correct levels of ERK activation for astroglial precursor RGCs to
94 translocate in appropriate numbers.

95 Heparan sulphate (HS), the carbohydrate component of cell surface and extracellular
96 matrix (ECM) heparan sulphate proteoglycans, is a negatively charged sulphated
97 polysaccharide that binds canonical FGFs in the ECM to regulate their movement and half-
98 life and also functions as an obligate FGF co-receptor in FGF:FGFR:HS ternary signalling
99 complexes on the cell surface (Balasubramanian and Zhang, 2016; Guillemot and Zimmer,
100 2011). HS biosynthesis is in two stages, Ext enzymes polymerise uronic acid – glucosamine
101 disaccharides making linear [uronic acid – glucosamine]$_n$ HS polymers which are then

JNeurosci Accepted Manuscript

102 modified by the enzymatic addition (by heparan sulphate sulphotransferases, HSTs) or
103 removal (by heparan sulphate sulphatases, Sulfs) of sulphate groups at specific positions on
104 the disaccharide residues. There are four classes of HST enzymes (Hs2st, Hs3st, Hs6st, and
105 Ndst) each adding sulphate to a specific position, for example Hs2st only adds sulphate to the
106 carbon atom in position 2 of uronic acid generating 2-O HS sulphation. While work in a
107 variety of systems shows that HS itself can play roles both in the transmission of FGF signals
108 through the ECM (non cell autonomous role) and the cellular response to FGF (cell
109 autonomous role) the potential for specific forms of HS sulphation to selectively regulate
110 FGFs by regulating the physical interaction between HS and FGF proteins is much less well
111 understood (Allen et al., 2001; Allen and Rapraeger, 2003; Balasubramanian and Zhang,
112 2016; Belenkaya et al., 2004; Chan et al., 2015; Chan et al., 2017; Christian, 2012; Guillemot
113 and Zimmer, 2011; Kinnunen et al., 2005; Loo et al., 2001; Loo and Salmivirta, 2002;
114 Makarenkova et al., 2009; Qu et al., 2011; Qu et al., 2012; Ramsbottom et al., 2014; Toyoda
115 et al., 2011; Yan and Lin, 2009; Yu et al., 2009; Zhang et al., 2012a).
116 The heparan sulphate code hypothesis states that different forms of HS sulphation can
117 encode specific instructions (Kreuger et al., 2006; Turnbull et al., 2001). In this study we
118 discover that 2-O HS sulphation catalysed by Hs2st functions non cell autonomously at the
119 developing telencephalic midline to supress FGF/ERK signalling that drives the somal
120 translocation of astroglial precursors required for normal CC development and present
121 evidence that Hs2st plays a selective role by modulating the physical interaction between
122 Fgf17 protein and HS and selectively supressing Fgf17 protein levels at the CSB.
123
124 **Materials and Methods**

125 **Animals**: All mice were bred in-house in line with Home Office UK legislation and licences
126 approved by the University of Edinburgh Ethical Review Committees and Home Office.
127 Embryos analysed in this study were of either sex. Animal husbandry was in accordance with
128 UK Animals (Scientific Procedures) Act 1986 regulations. The *Hs2st* LacZ (*Hs2st*$^{-}$) null
129 allele comprised a *LacZ* gene trap vector integrated into the *Hs2st* locus, the *Hs6st1*
130 LacZiresPLAP (*Hs6st1*$^{-}$) null allele comprised a *LacZiresPLAP* gene trap vector integrated in
131 the *Hs6st1* locus, both were genotyped by PCR as previously described (Bullock et al., 1998;
132 Conway et al., 2011; Pratt et al., 2006). For some *ex vivo* experiments *Hs2st*$^{-/+}$ mice were
133 crossed with mice carrying the TP6.3 Tau (τ) -GFP fusion transgene to generate *Hs2st*$^{-/-}$ and
134 *Hs2st*$^{+/+}$ embryos with *τGFP*$^{+}$ axons (Pratt et al., 2000). For conditional mutagenesis floxed

JNeurosci Accepted Manuscript

135 *Ext1* (*Ext1*^{fl}) or *Hs2st* (*Hs2st*^{fl}) alleles were combined with either *Zic4*^{Cre} (septal deletion) or
136 *Emx1*^{CreER} (cortical deletion) driver alleles (Inatani et al., 2003; Kessaris et al., 2006; Rubin et
137 al., 2010; Stanford et al.). *CreER* activity was induced at E9.5 by administering tamoxifen
138 (dissolved in corn oil using a sonicator) to pregnant dams by intraperitoneal (IP) injection
139 (120mg/kg dose). Lineages of cells in which Cre was active were visualised using a
140 Rosa26R-floxed-stop-EGFP reporter allele (Sousa et al., 2009).

141 ***Ex vivo* assays:** *Ex vivo* culture experiments were performed essentially as described
142 previously (Niquille et al., 2009) Explants were cultured on nucleopore polycarbonate
143 membranes (Whatman) floating on 1 ml 'Neurobasal media' (Neurobasal medium (Life
144 Technologies) supplemented with L-glutamine, glucose and penicillin/streptomycin) at 37°C
145 with 5% CO_2 in a humidified incubator. Brains were dissected from embryos in oxygenated
146 Earle's balanced salt solution (Life Technologies), embedded in low melting point agarose,
147 sliced using a vibratome (Leica VTS-1000), and transferred to Modified Eagle medium
148 (MEM, Life Technologies) with 5% foetal bovine serum for 1 hour. For CC axon navigation
149 assays 400μm thick E17.5 coronal slices incorporating the CC axon tract were prepared and
150 frontal cortex explants from τ-GFP^{+} slices were transplanted into the equivalent region in τ-
151 GFP^{-} slices prior to culturing in Neurobasal media for 72 hours, fixation in 4%
152 paraformaldehyde (PFA), and GFP immunofluorescence. For glial translocation experiments
153 10 mg/ml BrdU dissolved in PBS was injected IP into pregnant dams with E14.5 litters which
154 were sacrificed 1 hour later and 350μm coronal slices incorporating the CSB prepared for
155 culture. In Fgf17 bead experiments Affi-gel blue gel (Bio-rad) beads pre-soaked in 100μg/ml
156 recombinant Fgf17 protein (R&D systems) or 5mg/ml BSA (Sigma) overnight at 4°C were
157 implanted into the slice, one Fgf17 and one BSA bead on either side of the midline just below
158 the GW, and the MEM replaced with Neurobasal media. For the FGFi culture, MEM media
159 was replaced with Neurobasal media containing either 25μM SU5402, 0.1% DMSO (FGF
160 inhibitor (FGFi) treated) or 0.1% DMSO (control). Slices were cultured for 2 or 48 hours,
161 fixed in 4% PFA, and 10μm frozen sections prepared for immuno-detection or *in situ*
162 hybridisation. Glial migration out of the VZ towards the pial surface was quantified from
163 BrdU/Sox9 immunofluorescence micrographs by demarcating the basal edge of the VZ
164 (easily identified by Sox9 staining) with a line and counting the number of Sox9^{+};BrdU^{+} cells
165 which had crossed this line. This allowed us to count glial (Sox9^{+}) cells that had incorporated
166 BrdU (BrdU^{+}) when they were in the VZ before the start of the culture and subsequently
167 exited the VZ and migrated towards the midline over the 2 day culture period when the

JNeurosci Accepted Manuscript

168 cultures were exposed to experimental substances (SU5402, DMSO, Fgf17 protein, or BSA).
169 4 or 6 sections were quantified per slice moving rostrally from the most caudal section in
170 which the GW could be identified on both sides of the section.

171 **Immunodetection:** Embryonic mouse brains were removed and fixed in 4% PFA in PBS
172 overnight at 4°C, cryoprotected in 30% sucrose in PBS, embedded in OCT, and 10µm
173 coronal frozen sections cut using a cryostat (Leica). Immunohistochemistry was performed as
174 described previously (Clegg et al., 2014). Primary antibodies: goat anti-GFP (diluted 1/250,
175 Abcam); rabbit anti-Sox9 (1/500, Cell Signalling Technologies); rat anti-L1 (1/200,
176 Millipore); rabbit anti-GFAP (1/200 Dako); rabbit anti-Hs2st (1/50, Abcam ab103120); rabbit
177 anti-Fgf17 (1/1000, Abcam ab187982); and rabbit anti-pErk1/2 (1/200, Cell signalling).
178 Secondary antibodies; donkey anti-goat Alexa Fluor 488; donkey anti-rabbit Alexa Fluor
179 568; and goat anti-rat 568 (all used at a dilution of 1/200 and from Invitrogen). Fluorescently
180 labelled sections were counterstained with DAPI (Invitrogen). For Hs2st and pErk1/2
181 antibody staining goat anti-rabbit biotin secondary antibody (1/200, Vector Laboratories) was
182 used and staining was visualised using a standard avidin-biotin diaminobenzidine (DAB)
183 staining procedure. The Fgf17 immunofluorescence was performed using exactly the same
184 protocol as previously described for Fgf8 except that the Fgf8 antibody was replaced with the
185 Fgf17 antibody (Clegg et al., 2014; Toyoda et al., 2011). Briefly, slides were first washed in
186 acetone for permeabilisation, Rabbit Fgf17 antibody applied, and the TSA plus Fluorescence
187 System kit (Perkin Elmer) used for fluorescence detection.

188 ***In situ* Hybridisation:** *In situ* hybridisation was carried out on 10µm frozen sections as
189 previously described (Wallace and Raff, 1999) using digoxigenin-labelled riboprobes for
190 *Slit2* and *Fgf17* (Erskine et al., 2000; Xu et al., 1999).

191 **Imaging:** Fluorescent labelled sections were imaged using either a Leica AF6000
192 epifluorescence microscope coupled to a Leica DFC360 digital camera or a Nikon Ti: E
193 Inverted confocal microscope. DAB stained and in situ hybridised sections were imaged
194 using a Leica DLMB microscope coupled to a Leica DFC480 colour digital camera.

195 **Fgf17 protein quantification:** Fgf17 fluorescence was quantified from E14.5
196 *Hs2st*$^{+/+}$;*Hs6st1*$^{+/+}$, *Hs2st*$^{-/-}$ and *Hs6st1*$^{-/-}$ coronal sections that had been processed for Fgf17
197 immunofluorescence in parallel and imaged under identical conditions in parallel using the
198 same method as previously described for Fgf8 protein quantification (Chan et al., 2017). For
199 each section IMAGE J was used to measure mean fluorescence intensity in a 100 x 150 µm

JNeurosci Accepted Manuscript

200 box drawn at the CSB encompassing the Fgf17 expression domain. For each embryo
201 quantification was performed for three sections along the rostro-caudal axis and averaged.

202 **IG Sox9^{+} cell quantification:** Quantification of Sox9 immunofluorescent positive cells
203 (Sox9^{+} cells) in the IG region of E18.5 *Hs2st$^{fl/fl}$;Zic4^{Cre}*, *Hs2st$^{+/+}$;Zic4^{Cre}* *Hs2st$^{fl/fl}$;Emx1^{CreER}*,
204 and *Hs2st$^{+/+}$;Emx1^{CreER}* embryos were performed as previously described (Clegg et al.,
205 2014). A counting box measuring 200µm x 200µm was placed on images of coronal sections
206 at the midline with the top edge at the dorsal extent of Sox9^{+} cells at the IG and the numbers
207 of Sox9^{+} cells in the box counted. For each embryo quantification was performed for three
208 sections along the rostro-caudal axis and averaged.

209 **Western Blotting:** Western blotting was performed as previously described (Clegg et al.,
210 2014), primary antibodies: rabbit anti-Hs2st (1/500, Abcam ab103120) and mouse anti-β-
211 actin (1/5000, Abcam). Secondary antibodies: goat anti-mouse Alexa Fluor 680 (Invitrogen)
212 and goat anti-rabbit 800 (Li-Cor).

213 **Ligand and Carbohydrate Engagement (LACE) Assay:** LACE assay was performed as
214 previously described (Allen et al., 2001; Allen and Rapraeger, 2003; Chan et al., 2015).
215 Briefly, frozen sections were incubated in 0.05% $NABH_4$/PBS for 15 min. After several
216 washes in PBS, sections were incubated in 0.1M glycine at 4°C overnight. Some sections
217 were incubated with Heparitinase I (Seikagaku) before proceeding. All Fgf and Fgfr-Fc
218 proteins were purchased from R&D Systems. Sections were then treated with 1% BSA/TBS
219 solution for 10 min before incubation with 3 µM recombinant mouse Fgf17 and 9 µM
220 recombinant human Fgfr1a(IIIc)-Fc or 30nM recombinant mouse Fgf8b and 100nM
221 recombinant human Fgfr3 (IIIc)-Fc at 4°C overnight. Fgf17 or Fgf8 were omitted from some
222 assays. Fluorescent LACE signal was generated by incubation with 1/200 anti-human IgG
223 (Fc-specific) Cy3 (Sigma) in 1% BSA/TBS. *Hs2st$^{+/+}$;Hs6st1$^{+/+}$*, *Hs2st$^{-/-}$* and *Hs6st1$^{-/-}$*
224 material that had been processed for each LACE assay condition in parallel were imaged
225 under identical conditions in parallel. For each section IMAGE J was used to measure mean
226 fluorescence intensity in a 100 x 150 µm box drawn encompassing the CSB. Background
227 signal was quantified from control LACE experiments from which the FGF ligand was
228 omitted and these values used for background subtraction. For each embryo quantification
229 was performed for three sections along the rostro-caudal axis and averaged.

230 **Data analysis and statistics:** Results are expressed as mean ±SEM. The statistical test and
231 sample size (n) for each experiment are specified in the figure legends. Statistical comparison

JNeurosci Accepted Manuscript

232 between 2 groups was performed with a t-test. Statistical comparison between > 2 groups was
233 performed with ANOVA followed by post-hoc t-test. $p < 0.05$ was considered significant.

234 **Results**

235 **Hs2st protein is widely expressed in the developing cerebral cortex and at the**
236 **telencephalic midline.**

237 In order to establish potential sites of action of Hs2st in CC development we first
238 examined the distribution of cells expressing Hs2st protein and contributing to developing
239 CC structures using Hs2st immunohistochemistry at E14.5 (Fig 1 A-D) and E18.5 (Fig 1 E-
240 M) spanning the period of CC axon tract development. Macroscopically, Hs2st protein
241 distribution closely resembles the *Hs2st-LacZ* reporter staining previously reported with
242 widespread Hs2st expression in the developing cerebral cortex and at the CSB at both E14.5
243 and E18.5 (Fig 1A,E, boxed areas indicate regions shown at higher magnifications in B-D
244 and F-M) (Conway et al., 2011). Subcellularly the Hs2st signal is punctate consistent with the
245 expected localisation of Hs2st in the Golgi apparatus (arrows point to Hs2st^{+} puncta in higher
246 magnification insets in Fig 1B,F,P). At E14.5 there was a high density of Hs2st^{+} puncta at the
247 CSB in the GW region where IG astroglial RGC prescursors reside (Fig 1B with boxed area
248 shown as higher magnification inset with arrows indicating Hs2st^{+} puncta) with the density
249 falling towards the pial surface although Hs2st^{+} puncta were visible. There were many Hs2st^{+}
250 puncta in the VZ of the cerebral cortex (Fig 1C) and also in the cortical plate (Fig 1D)
251 indicating that many cortical progenitors and post-mitotic neurones express Hs2st. At E18.5
252 Hs2st is expressed by many cells in the IG (Fig 1F) and at the apical surface of the ventricular
253 zone (VZ) at the GW (Fig 1G), septum (Fig 1H), and ventral telencephalon (Fig 1I) with the
254 number of Hs2st expressing VZ cells diminishing as distance from the ventricle increases. In
255 the cerebral cortex Hs2st is expressed by many cells close to the apical surface of the VZ (Fig
256 1J). Large numbers of post-mitotic cortical neurons outside the VZ express Hs2st and moving
257 towards the pial suface the density of Hs2st^{+} puncta varies with laminar position (compare
258 Fig 1 K,L,M showing relatively high Hs2st^{+} puncta density in cortical layers adjacent to the
259 pial membrane (M) and in the intermediate zone (K) and lower density in the intervening
260 region (L)). We validated the Hs2st antibody by demonstrating absence of the punctate
261 Hs2st^{+} immunostaining in *Hs2st*$^{-/-}$ embryonic material (compare Fig 1N,P to O,Q – note that
262 the more diffuse staining persists in *Hs2st*$^{-/-}$ tissue and we discounted this as non-specific
263 background) and western blot showing that the predicted 42kDa Hs2st protein band was
264 present in *Hs2st*$^{+/+}$ and absent from *Hs2st*$^{-/-}$ telencephalic protein extracts (Fig 1R). To

JNeurosci Accepted Manuscript

conclude, Hs2st protein is present in developing cerebral cortex, the source of CC axons, as well as in progenitor and post-mitotic cells of the CSB region constituting the environment through which midline crossing CC axons navigate. The Hs2st expression analysis suggests multiple potential sites of action for 2-O HS sulphation in CC development.

The *Slit2* expressing IG is expanded in *Hs2st*$^{-/-}$ embryos.

We previously reported that increased numbers of astroglia at the pial surface of the *Hs2st*$^{-/-}$ CSB stemmed from precocious glial translocation and found no evidence that changes in cell proliferation or death contributed to this phenotype (Clegg et al., 2014; Conway et al., 2011). In order to determine whether there is an expansion of the IG in *Hs2st*$^{-/-}$ embryos we compared the expression of *Slit2* mRNA, a marker of GW and IG glia but not MZ glia, between *Hs2st*$^{+/+}$ and *Hs2st*$^{-/-}$ embryos at E16.5 (Shu and Richards, 2001; Shu et al., 2003). In *Hs2st*$^{+/+}$ embryos *Slit2*$^{+}$ cells form a compact focus at the IG that increases in size moving caudally (Fig 2 A,C,E – *Slit2* expression domain at IG indicated by brackets). In *Hs2st*$^{-/-}$ embryos the Slit2 expression domain is greatly expanded at the pial surface along the rostro-caudal axis (Fig 2 B,D,F – expanded *Slit2* expression domain indicated by brackets). We conclude that an expansion of the *Slit2*$^{+}$ IG astroglial population makes a major contribution to the *Hs2st*$^{-/-}$ phenotype.

Cell autonomy of HS and 2-O HS sulphation in astroglial precursor somal translocation and corpus callosum development.

We next exploited conditional mutagenesis of *Hs2st* or *Ext1* to experimentally uncouple specific functions of 2-O sulphation from more general functions of HS in astroglial precursor translocation and corpus callosum development. Widespread expression of HS and 2-O HS sulphation leaves open the possibility that each regulates GW→IG astroglial precursor somal translocation cell autonomously by modulating the response to signals, non cell autonomously by regulating the supply of signals, or both. To resolve this we identified two *Cre* alleles, *Zic4*^{Cre} and *Emx1*^{CreER}, that drive *LoxP* mediated mutagenesis in the astroglial lineage or in their cellular environment respectively and used them to conditionally ablate either HS (*Ext1*^{LoxP} mutagenesis) or 2-O HS sulphation (*Hs2st*^{LoxP} mutagenesis) to test for cell autonomous or non cell autonomous functions. We refer to these as '*Zic4* lineage' and '*Emx1* lineage' and next present their characterisation using a floxed-stop GFP reporter that turns on GFP expression in *Cre* expressing cells and their descendants before describing experiments where they are employed to conditionally generate loss of function mutations in

JNeurosci Accepted Manuscript

299 *Ext1^{Fl}* or *Hs2st^{Fl}* alleles (Inatani et al., 2003; Kessaris et al., 2006; Rubin et al., 2010; Sousa
300 et al., 2009; Stanford et al.).
301
302 **Characterisation of *Zic4* and *Emx1* lineages.**
303 The septum is of *Zic4* lineage, as shown by strong expression of the GFP reporter (Fig
304 3A). The GFP signal in the intermediate zone of the cerebral cortex (asterisks, Fig. 3A) is due
305 to GFP$^+$ thalamocortical axons that project from *Zic4* lineage cells in the thalamus and cells
306 of sub-cortical origin as previously reported (Rubin et al., 2010). At the midline GFP$^+$ cells of
307 the *Zic4* lineage are predominantly located ventral to the CSB (dashed lines in Fig 3B) but
308 there is also GFP expression in the IG (boxed area 'D' in Fig 3B). Sox9 is a transcription
309 factor that marks the nuclei of RGCs in the VZ and differentiated astroglia in the IG and
310 MZG and we previously showed that the positioning of Sox9$^+$ cells is of critical importance
311 for the development of the CC (Clegg et al., 2014). Combining GFP with Sox9
312 immunostaining reveals the contribution of the *Zic4* lineage to the CSB astroglial
313 populations. There is a sharp boundary (dashed line in Fig 3C) in the VZ of the CSB between
314 Sox9$^+$;GFP$^+$ cells (arrowheads in Fig 3C) on the septal side and Sox9$^+$;GFP$^-$ cells (arrows in
315 Fig 3C) on the cortical side. Virtually all the Sox9$^+$ cells in the IG (Fig 3D) and MZG (fig 3E)
316 are also GFP$^+$ (arrowheads in Fig 3D,E) indicating that these cells are *Zic4* lineage. These
317 data show that the *Zic4* lineage contributes Sox9$^+$ cells to the septal VZ and strikingly is the
318 sole source of Sox9$^+$ astroglia in the IG (Fig 3F).
319 To mark the *Emx1* lineage, tamoxifen was administered to *Emx1^{CreER}* embryos
320 harbouring the floxed-stop GFP reporter at E9.5 so that early *Emx1* expressing cerebral
321 cortex progenitors and their descendants were rendered GFP$^+$. Examination of the expression
322 of the GFP reporter shows that, as expected, the developing cerebral cortex and CC axons are
323 of *Emx1* lineage (Fig. 3G) and that at the midline GFP expression is predominantly located
324 dorsal to the CSB (dashed lines in Fig 3H). Higher magnification shows that there is a sharp
325 boundary between GFP$^+$ and GFP$^-$ cells at the VZ of the CSB (dashed line in Fig 3I).
326 Combining Sox9 and GFP immunostaining reveals the contribution of the *Emx1* lineage to
327 *Sox9*$^+$ cells. Sox9$^+$;GFP$^+$ cells (arrowheads in Fig 3I) populate the VZ on the cortical side of
328 the boundary with Sox9$^+$;GFP$^-$ cells on the septal side (arrows in Fig 3I) showing that the
329 *Emx1* lineage contributes Sox9$^+$ cells exclusively to the cortical side of the VZ. All Sox9$^+$
330 cells in the IG (Fig 3J) and MZ (Fig 3K) are GFP$^-$ (arrows in Fig 3J,K) indicating that the
331 *Emx1* lineage does not contribute Sox9$^+$ cells to the IG. These data show that the *Emx1*

JNeurosci Accepted Manuscript

332 lineage contributes $Sox9^+$ cells to the cortical VZ but no cells of this lineage contribute $Sox9^+$
333 astroglia to the IG (schema in Fig 3L).
334
335 ***Ext1* is required by both *Emx1* and *Zic4* lineage cells for corpus callosum development.**
336 To determine the cellular requirement for HS we deleted *Ext1*, essential for HS
337 synthesis, in the *Zic4* or *Emx1* lineages. In control embryos L1 immunostaining labels axons
338 in the U-shaped CC while GFAP staining labels midline astroglial structures (Fig. 4A with
339 higher magnification of IG and GW in Fig 4D,G). Removing HS from either the *Zic4* lineage
340 (Fig 4B with higher magnification of IG and GW in Fig 4E,H) or the *Emx1* lineage (Fig 4C
341 with higher magnification of IG and GW in Fig 4F,I) generates a severe CC agenesis
342 phenotype ($Zic4^{Cre};Ext1^{Fl/Fl}$ n=4/4; $Emx1^{CreER};Ext1^{Fl/Fl}$ n=3/3). In *Emx1* conditional mutants
343 ($Emx1^{CreER};Ext1^{Fl/Fl}$) CC axons fail to cross the midline and form Probst bundles (P) some
344 distance short of the midline (Fig. 4B). $GFAP^+$ astroglial cells are present in the IG (Fig 4E)
345 and at the GW (fig 4H) in a pattern grossly similar to that of controls (compare Fig. 4D,G to
346 E,H). In *Zic4* conditional mutants ($Zic4^{Cre};Ext1^{Fl/Fl}$) CC axons approach the midline but fail
347 to cross (Fig. 4C with higher magnification of IG and GW in Fig 4F,I). Astroglial populations
348 in *Zic4* conditional mutants are obviously disrupted with less intense GFAP staining at the
349 midline (compare IG region in Fig 4 D to F) and more GFAP at the GW than in controls
350 (arrows in Fig 4I, compare Fig. 4G to I) suggesting that in these embryos astroglial
351 precursors translocate less efficiently to the IG and instead remain in the GW. We noted that
352 the cerebral cortex of $Zic4^{Cre};Ext1^{Fl/Fl}$ brains was thinned and the ventricles were enlarged
353 (compare Fig4 A to C), this hydrocephalus-like phenotype is intriguing because the cerebral
354 cortex is not of the *Zic4* lineage indicating a non-cell autonomous mechanism by which HS
355 regulates cerebral cortex development. The FGFR1/ FGF2 ligand and carbohydrate
356 engagement (LACE) assay detects endogenous HS on tissue sections by forming ternary
357 complexes with exogenously added FGF2 and FGFR1 (red LACE signal in Fig 4 J-O) (Allen
358 et al., 2001; Chan et al., 2015). HS is ubiquitously expressed in both cortical and septal
359 compartments of control telencephalon (Fig 4J, higher magnification of CSB in M) and, as
360 intended, HS synthesis is blocked in the cortex and cortical axons of $Emx1^{CreER};Ext1^{Fl/Fl}$
361 embryos (Fig 4K, CSB shown at higher magnification in N with arrows indicating HS
362 deficient cortical region) and in the septum of $Zic4^{Cre};Ext1^{Fl/Fl}$ embryos (Fig 4L, higher
363 magnification of CSB in O with arrows indicating HS deficient septum). Predigesting tissue
364 sections with heparitinase eliminated the LACE signal (not shown) confirming specificity of
365 this assay for detecting HS. The salient conclusions from the *Ext1* conditional mutagenesis

for the current study are that HS is indispensable from both the *Zic4* and the *Emx*1 lineages for CC development and that removing HS from the *Zic4* lineage inhibits *Zic4* lineage astroglia reaching the IG region.

***Hs2st* is required by *Emx1* lineage but not *Zic4* lineage cells for corpus callosum development.**

Having established that both *Zic4* and *Emx1* lineages need to synthesise HS for normal CC development we next asked whether 2-O HS sulphation of the HS is required in either lineage. Hs2st is the sole enzyme capable of imparting 2-O HS sulphation onto HS so to determine the cellular requirement for 2-O HS sulphation we deleted *Hs2st* in the *Zic4* or *Emx1* lineages. Control *Hs2st*$^{+/+}$ genotypes (*Hs2st*$^{+/+}$*;Emx1*^{CreER} and *Hs2st*$^{+/+}$*;Zic4*^{Cre}) displayed neither CC agenesis nor midline astroglial disorganisation, the control embryo shown in Fig 5 (A,D,G,J – D,G reproduced from Fig 3 H,J) is *Hs2st*$^{+/+}$*;Emx1*^{CreER} genotype. The CC and the midline astroglial structures form normally in *Hs2st*$^{fl/fl}$*;Zic4*^{Cre} conditional mutants and the organisation of L1^{+} axons and GFAP^{+} astroglia are indistinguishable from control embryos (6/6 embryos) (Fig. 5B, compare to control in 5A). The organisation of GFP^{+} *Zic4* lineage cells is the same in *Hs2st*$^{fl/fl}$*;Zic4*^{Cre} embryos as in *Hs2st*$^{+/+}$*;Zic4*^{Cre} embryos (compare Fig 5E,H to Fig 3B,D) and IG Sox9^{+} cell counts confirm that the numbers of Sox9^{+} cells in the IG are not significantly different to control *Hs2st*$^{+/+}$ embryos (Fig 5M, compare blue and orange bars) indicating no cell autonomous requirement for *Hs2st* in the *Zic4* lineage Sox9^{+} IG astroglia. To exclude the possibility of a compensatory mechanism by which the *Hs2st*$^{fl/fl}$*;Zic4*^{Cre} IG is populated by *Hs2st*$^{+/+}$ cells from a different lineage we performed Hs2st immunohistochemistry and confirmed that Hs2st expression is indeed absent from all cells in the IG (Fig 5K, note this is an adjacent section from the same embryo to the one shown in 5H). In *Hs2st*$^{fl/fl}$*;Emx1*^{CreER} embryos the CC fails to form in approximately 50% of cases, embryos either had a severe phenotype (Fig 5C, 5/9 embryos) or appeared completely unaffected (Fig 5C', 4/9 embryos). CC axons form Probst bundles (P) on either side of the telencephalic midline while the GFAP^{+} IG is expanded (asterisks, Fig. 5C). The anatomy and incomplete penetrance of the CC phenotype in *Hs2st*$^{fl/fl}$*;Emx1*^{CreER} embryos closely resemble constitutive null *Hs2st*$^{-/-}$ embryos indicating that *Hs2st* function within the *Emx1* lineage is sufficient for normal CC development (Clegg et al., 2014; Conway et al., 2011). As in control *Hs2st*$^{+/+}$*;Emx1*^{CreER} embryos (Fig 5 D,G) the GFP and Sox9 signals did not overlap in the IG region of control or *Hs2st*$^{fl/fl}$*;Emx1*^{CreER} embryos (Fig 5F, boxed area shown at higher magnification in 5I) and the Sox9^{+} cells in the IG of control

JNeurosci Accepted Manuscript

JNeurosci Accepted Manuscript

embryos and the expanded IG of *Hs2st*$^{fl/fl}$;*Emx1*^{CreER} embryos were GFP$^-$ (arrows in Fig 5I indicate Sox9$^+$;GFP$^-$ cells). Counts of Sox9$^+$ cells confirmed a significant increase in the IG of affected *Hs2st*$^{fl/fl}$;*Emx1*^{CreER} embryos compared to controls (Fig 5M, compare blue and purple bars). Immunostaining for Hs2st on adjacent sections confirmed that IG cells in *Hs2st*$^{fl/fl}$;*Emx1*^{CreER} embryos retain Hs2st protein expression (Fig 5L). Because Sox9$^+$ IG astroglia do not belong to the *Emx1* lineage their ectopic position in *Hs2st*$^{fl/fl}$;*Emx1*^{CreER} embryos, despite retaining *Hs2st* function, allows us to conclude a cell non autonomous requirement for Hs2st in the translocation of astroglial precursors to the IG..

The salient conclusions from these conditional mutagenesis experiments are that while the *Zic4* lineage astroglia do require *Ext1* to form midline astroglial structures they do not require *Hs2st*, strongly suggesting that while these *Zic4* lineage cells require HS on their cell surface to respond to translocation signals there is no need for the HS to be 2-O sulphated. In contrast *Hs2st* is absolutely required in the surrounding *Emx1* lineage cells indicating a non cell autonomous mechanism by which 2-O HS sulphation controls the transmission of translocation signals to the *Zic4* lineage astroglial precursors.

_Hs2st_ is not required cell autonomously by CC axons to navigate the midline.

The conditional mutagenesis experiments showed that Hs2st has a non cell autonomous role in GW→IG somal translocation, but, because Hs2st is expressed throughout the cerebral cortex, did not resolve whether there is an additional cell autonomous requirement in CC axon navigation. To answer this we performed *ex vivo* transplant experiments in which cerebral cortical tissue from transgenic mice ubiquitously expressing τGFP, which efficiently labels axons of τGFP$^+$ cells, was transplanted into τGFP$^-$ telencephalic slices containing the CC axon pathway and CSB structures (Niquille et al., 2009; Pratt et al., 2000). When *wild-type* (*WT*) E17.5 τGFP$^+$ cortical explants are transplanted into age matched τGFP$^-$ *WT* cortical slices τGFP$^+$ axons extend across the telencephalic midline forming the characteristic U-shape of the CC and reach the cortex of the opposite hemisphere (n=3/3 cultures, arrows in Fig 6A,D point to crossing axons). When *Hs2st*$^{-/-}$ τGFP$^+$ cortical explants are transplanted into τGFP$^-$ *WT* slices, axons are able to cross the midline to reach the opposite hemisphere in a manner indistinguishable from that seen in the *WT*→*WT* transplants (n=4/4 cultures, arrows in Fig 6B,E point to crossing axons). In contrast, when τGFP$^+$ *WT* cortical explants are transplanted into τGFP$^-$ *Hs2st*$^{-/-}$ slices axons are unable to reach the opposite cortical hemisphere and instead remain within the cingulate cortex or invade the septum (n=6/6 cultures), resembling the *in vivo* CC phenotype observed

JNeurosci Accepted Manuscript

in *Hs2st*$^{-/-}$ embryos (Clegg et al., 2014; Conway et al., 2011). Note that in all cultures a few axons grew into the septum (arrowheads in Fig 6 D,E,F). Schematics summarising these experiments are shown in Fig 6 G,H,I. These data show 2-O HS sulphation is not required cell autonomously by CC projection neurons for axon guidance across the midline strongly suggesting that disorganisation of midline guidepost astroglial cells is the primary cause of the *Hs2st*$^{-/-}$ CC agenesis phenotype.

Abnormally high FGF/ERK signalling causes the *Hs2st*$^{-/-}$ precocious astroglial translocation phenotype.

We previously reported a correlation between hyperactive ERK signalling at the CSB and precocious somal translocation of astroglia to the midline in *Hs2st*$^{-/-}$ embryos but we did not formally establish that this stemmed from hyperactive FGF/ERK signalling (Chan et al., 2017; Clegg et al., 2014). To address this we employed an *ex vivo* assay in which coronal *WT* or *Hs2st*$^{-/-}$ telencephalic slices incorporating the CSB were cultured on floating membranes for long enough to allow somal translocation to the midline and attempted to rescue the *Hs2st*$^{-/-}$ phenotype by pharmacological abrogation of FGF/ERK signalling. *WT* or *Hs2st*$^{-/-}$ E14.5 slices were cultured in the presence of the Fgfr1 inhibitor SU5402 dissolved in DMSO (FGFi treatment) to inhibit FGF/ERK signalling or in DMSO alone (untreated control) for 48hr (Fig 7A). To aid subsequent identification of translocating cells, a subpopulation RGCs undergoing S-phase in the VZ at E14.5 were labelled just prior to culturing with a single pulse of BrdU. Immunohistochemistry for pErk (brown stain in Fig 7 B,D,F,H) confirms inhibition of FGF/ERK signalling in both FGFi treated *WT* and *Hs2st*$^{-/-}$ cultures (Fig 7D,H) compared to untreated cultures (Fig 7B,F) showing that FGF signalling through Fgfr1 accounts for ERK phosphorylation in both genotypes so, importantly, demonstrating that ERK hyperactivation in *Hs2st*$^{-/-}$ embryos does not stem from an FGF-independent mechanism for ERK activation (Chan et al., 2017; Clegg et al., 2014). After 48 hours some Sox9$^+$ cells (red) had left the VZ and translocated to the midline in untreated *WT* cultures (arrow in Fig 7C) with many more populating the midline in untreated *Hs2st*$^{-/-}$ cultures (arrow in Fig 7G) validating that our *ex vivo* assay replicates the *in vivo Hs2st*$^{-/-}$ phenotype. Consistent with our hypothesis, FGFi treatment of both *WT* and *Hs2st*$^{-/-}$ cultures resulted in a large decrease in Sox9$^+$ cells reaching the midline (compare Fig 7E,I to C,G). We quantified glial translocation by counting the numbers of Sox9$^+$ cells born in the VZ at E14.5 (Sox9$^+$;BrdU$^+$ cells, yellow – inset in Fig 7 C,E,G,I shows higher magnification) that had exited the VZ towards the midline (VZ demarcated by dotted line in Fig 7 C,E,G,I) after 2 days in culture. Counts of

JNeurosci Accepted Manuscript

468 BrdU^{+};Sox9^{+} cells showed that glial translocation was significantly greater in *Hs2st*$^{-/-}$
469 compared to *WT* cultures along the rostro-caudal axis (dark purple and green lines in Fig 7J)
470 and in both cases almost completely suppressed by FGFi treatment (pale purple and green
471 lines in Fig 7J).

472 We conclude that the precocious glial translocation phenotype in H*s2st*$^{-/-}$ embryos is
473 caused by hyperactive FGF/ERK signalling from E14.5 onwards. Taken together with our
474 *Hs2st* conditional mutagenesis experiments demonstrating a non cell autonomous role for
475 *Hs2st* in astroglial precursor translocation we hypothesise that Hs2st normally suppresses the
476 supply of FGF proteins to translocation competent astroglial precursors in the GW.
477
478

479 ***Hs2st* suppresses Fgf17 protein levels.**

480 We next sought to identify an FGF protein that is targeted by *Hs2st*. Despite its well
481 known role in CC development Fgf8 protein levels are not significantly increased at the CSB
482 of *Hs2st*$^{-/-}$ embryos forcing us to consider other FGFs (Chan et al., 2017; Clegg et al., 2014).
483 A promising candidate is *Fgf17*, a member of the *Fgf8* subfamily transcribed at the CSB in a
484 similar pattern to *Fgf8* (Cholfin and Rubenstein, 2008; Zhang et al., 2012b). Fgf17 is a
485 canonical FGF that binds to HS, so is potentially regulated via its interaction with HS, and is
486 known to play a role in patterning the telencephalon although its role in CC development has
487 not been fully characterised (Cholfin and Rubenstein, 2007; Hoch et al., 2015; Li and
488 Kusche-Gullberg, 2016). We hypothesised that Hs2st normally suppresses Fgf17 protein and
489 predicted that Fgf17 protein levels would be increased at the *Hs2st*$^{-/-}$ CSB. We compared the
490 expression of Fgf17 protein in the developing CSB of *WT* and *Hs2st*$^{-/-}$ embryos at three
491 developmental stages (E12.5, E14.5, and E16.5), spanning the interval of midline glial
492 translocation (Fig 8$A_{1,2}$-$H_{1,2}$). At E12.5 telencephalic Fgf17 protein is restricted to the CSB
493 region with no obvious difference between *WT* and *Hs2st*$^{-/-}$ (compare Fig 8 A_1,B_1 to A_2,B_2).
494 By E14.5 there is an expanded Fgf17 protein domain at the CSB of *Hs2st*$^{-/-}$ embryos
495 (compare Fig 8 D_1,E_1 to D_2,E_2, * in E_2 marks the expanded Fgf17 protein domain).
496 Quantification of Fgf17 immunofluorescence shows a significant ~2 fold increase in Fgf17
497 protein levels in this region of *Hs2st*$^{-/-}$ CSB (Fig 8W – compare blue and green bars). At
498 E16.5 Fgf17 protein is much closer to detection threshold than at the earlier stages in both
499 genotypes (Fig 8$G_{1,2}$,$H_{1,2}$) although the increased protein spread in the mutant persists (* in
500 Fig 8H_2) indicating that the *Hs2st*$^{-/-}$ CSB is exposed to a prolonged overdose of Fgf17 protein
501 spanning E14.5-E16.5. We next examined *Fgf17* mRNA at the CSB so see whether the

JNeurosci Accepted Manuscript

502 increase in Fgf17 protein in *Hs2st*$^{-/-}$ CSB was underpinned by altered *Fgf17* gene expression.
503 There was no evidence for this at E12.5 or E14.5 where *Fgf17* mRNA expression pattern
504 remains similar between *Hs2st*$^{+/+}$ and *Hs2st*$^{-/-}$ embryos (compare Fig 8 C_1 to C_2 and F_1 to F_2),
505 however, the expression domain of *Fgf17* mRNA is increased in E16.5 *Hs2st*$^{-/-}$ CSB
506 (compare Fig 8I_1 to I_2, * in I_2 marks expanded *Fgf17* mRNA domain). This subsequent
507 increase in *Fgf17* mRNA in the E16.5 *Hs2st*$^{-/-}$ CSB indicates that the *Hs2st*$^{-/-}$ phenotype has a
508 transcriptional component or that there are more cells expressing *Fgf17* mRNA in the
509 expanded *Hs2st*$^{-/-}$ IG although this cannot be the primary event as it is not apparent at E14.5,
510 the stage at which we previously identified precocious astroglial precursor translocation was
511 well underway in *Hs2st*$^{-/-}$ embryos (Clegg et al., 2014).

512 Mosaic analysis (Fig 5) indicated that *Hs2st* function in the *Emx1* lineage negatively
513 regulates a signal promoting GW→IG translocation of *Zic4* lineage glial cells by a non cell
514 autonomous mechanism and Fgf17 expression analysis (Fig 8) makes Fgf17 a strong
515 candidate for the signal. Based on this we hypothesised that Fgf17 is expressed in cells
516 surrounding the *Zic4* lineage cells and performed detection of *Fgf17* mRNA or protein in
517 E14.5 WT embryos in which the *Zic4* lineage is labelled GFP$^+$. *Fgf17* mRNA is expressed at
518 the GW and the IG (Fig 8J) and higher power magnification shows that in the VZ GFP$^+$ cells
519 express little if any *Fgf17* mRNA and conversely cells expressing the highest levels of *Fgf17*
520 mRNA are GFP$^-$ (Fig 8 K_{1-3}, arrows indicate GFP$^+$ cell location). This complementarity
521 between Fgf17 mRNA expressing and *Zic4* lineage cells is preserved at the IG (Fig 8L_{1-3},
522 arrows indicate GFP$^+$ cell location). Fgf17 protein predominates at the IG (Fig 8M) and
523 higher power magnification shows that while Fgf17 protein is barely detectable at the GW
524 (Fig 8N_{1-3}) there are a number of much higher Fgf17 expressing cells at the IG and these cells
525 are GFP$^-$ confirming that they do not belong to the *Zic4* lineage (Fig 8O_{1-3}, arrows indicate
526 GFP$^+$ cell location). Interestingly, although cells in the GW and IG express comparable levels
527 of *Fgf17* mRNA (compare Fig 8K_1 to L_1) the expression of Fgf17 protein is much higher in
528 the IG (compare Fig 8N_1 to O_1) suggesting a post-transcriptional repression selectively at the
529 GW. Our identification of Hs2st as a repressor of Fgf17 protein levels at this stage makes
530 Hs2st a strong candidate, indeed, closer examination of *Hs2st* expression using the *Hs2st-*
531 *LacZ* reporter shows that Hs2st is expressed in a GW^{High}-IG^{Low} pattern (Fig 8P, also apparent
532 in the Hs2st immunohistochemistry (Fig 1B)), complementary to the GW^{Low}-IG^{High} Fgf17
533 protein distribution. Together these data bolster the idea that Hs2st acts to suppress Fgf17
534 protein supply to *Zic4* lineage cells by a post-transcriptional mechanism.

JNeurosci Accepted Manuscript

535 We conclude that Hs2st primarily supresses the level and spread of Fgf17 protein
536 emanating from the *Emx1* lineage in the CSB.
537
538 ***Hs6st1* does not affect Fgf17 protein levels.**
539 We next addressed whether the ability of 2-O HS sulphation to supress Fgf17 protein
540 levels *in vivo* represented a specific function of Hs2st or was redundant with other HSTs. We
541 chose to examine Hs6st1, an HST that catalyses 6-O HS sulphation, because we have
542 previously shown that *Hs6st1* (but not *Hs2st*) supresses levels of the closely related Fgf8
543 protein at the CSB *in vivo* (Chan et al., 2017; Clegg et al., 2014). However, we were unable
544 to detect increased expression of Fgf17 protein (compare Fig 8 Q_1, R_1 to Q_2, R_2 and T_1, U_1 to
545 T_2, U_2) or *Fgf17* mRNA (compare Fig 8S_1 to S_2 and V_1 to V_2) in *Hs6st1*$^{-/-}$ compared to wild-
546 type CSB at either E14.5 or E16.5. Quantification of Fgf17 immunofluorescence shows
547 unchanged Fgf17 protein levels in this region of *Hs6st1*$^{-/-}$ CSB (Fig 8W – compare blue and
548 purple bars). These data demonstrate that the negative relationship between *Hs2st* and *Fgf17*
549 is selective *in vivo* because it does not apply to *Hs6st1*.
550
551 **Exogenously applied Fgf17 phenocopies the *Hs2st*$^{-/-}$ astroglial translocation phenotype.**
552 Our data suggest that the *Hs2st*$^{-/-}$ phenotype stems from abnormally high levels of
553 Fgf17 protein at the CSB causing FGF/ERK hyperactivation and precocious somal
554 translocation to the IG. This requires that *Hs2st*$^{-/-}$ CSB cells are competent to respond to
555 Fgf17 protein and that application of ectopic Fgf17 triggers precocious glial translocation,
556 neither of which have been previously established. We redeployed the CSB *ex vivo* culture
557 assay (see Fig 7) with the modification that beads soaked in either recombinant Fgf17 protein
558 (Fgf17 treatment) or in BSA (control) were implanted into coronal slices of CSB region on
559 either side of the midline (Fig 9A). *WT* or *Hs2st*$^{-/-}$ slices implanted with Fgf17 and BSA
560 beads were cultured for 2 hours before processing for Fgf17 (green signal) and pErk (red
561 signal) double immunofluorescence (Fig 9B). In both *WT* and *Hs2st*$^{-/-}$ cultures Fgf17 protein
562 was detectable adjacent to the edge of the bead (green signal) and this activated ERK
563 phosphorylation in a similar pattern (red signal) with no obvious differences between *WT* and
564 *Hs2st*$^{-/-}$ indicating that *Hs2st*$^{-/-}$ CSB tissue is competent to respond to Fgf17 (Fig. 9B top
565 row). The lack of Fgf17 or pERK signal in the BSA control (Fig 9B, bottom row) confirms
566 Fgf17 antibody specificity and that pERK activation was specifically induced by exogenously
567 applied Fgf17. We performed Sox9/BrdU analysis (exactly as described above for the FGFi
568 experiments - Fig 7) to assess the impact of experimentally introduced Fgf17 on astroglial

JNeurosci Accepted Manuscript

569 translocation to the midline after 48 hours in culture. The results were dramatic, the side with
570 the Fgf17-bead showed many more $Sox9^+$ (red) cells in the IG region (large arrow on right
571 side of Fig 9C) than the side with the BSA bead (smaller arrow on left side of Fig9C).
572 Quantification of $Sox9^+$;$BrdU^+$ (yellow) cells (Fig 9D shows higher magnification of IG
573 region) confirmed a significant increase in astroglial translocation to the midline along the
574 rostro-caudal axis on the side exposed to Fgf17 (Fig 9E, compare green (Fgf17) to black
575 (control) lines). An important function of IG glia is to secrete Slit2 and repulsively guide CC
576 axons in the correct trajectory across the midline. At E16.5 *Slit2* mRNA is normally
577 expressed in the IG region and in *Hs2st*$^{-/-}$ embryos the midline *Slit2* expression domain is
578 expanded (compare Fig 2C,E to D,F – *Slit2* expression domain bracketed). Experimentally
579 introduced Fgf17 is sufficient to phenocopy this aspect of the *Hs2st*$^{-/-}$ phenotype in our *ex*
580 *vivo* assay as the side exposed to the Fgf17 bead has a much larger *Slit2* domain than the BSA
581 treated side (compare left (Fgf17) and right (control) bracketed areas in Fig 9F) consistent
582 with precocious translocation of excessive numbers of *Slit2*$^+$ IG glia.

583 We conclude that *Hs2st*$^{-/-}$ CSB tissue is competent to respond to Fgf17 protein and
584 abnormally high levels of Fgf17 protein are sufficient to phenocopy the *Hs2st*$^{-/-}$ astroglial
585 translocation phenotype consistent with the model presented in Fig 10.

586

587 ***Hs2st* selectively facilitates physical interaction between Fgf17 protein and HS.**

588 Our *in vivo* data show that Hs2st suppresses the levels of Fgf17 protein and that this
589 represents a selective interaction between Hs2st mediated 2-O HS sulphation and Fgf17
590 protein levels *in vivo* because Hs2st does not suppress the levels of the closely related Fgf8
591 protein while Hs6st1, which catalyses 6-O HS sulphation, does not suppress Fgf17 protein
592 levels (Chan et al., 2017; Clegg et al., 2014), Fig 8). These *in vivo* experiments do not
593 however resolve whether differential sulphation has a correspondingly direct selective effect
594 on the physical interaction between HS and Fgf17. In order to test the hypothesis that Hs2st
595 has a selective effect on the binding of Fgf17 protein to HS molecules we turned to a
596 biochemical assay, the ligand and carbohydrate engagement (LACE) assay, that probes
597 physical interaction between HS and FGF proteins by quantifying the ability of endogenous
598 HS in tissue sections to form Fgf:Fgfr:HS complexes with exogenously added Fgf protein
599 and Fgfr ectodomain fused to an Fc tag for immunofluorescent detection (Allen et al., 2001;
600 Chan et al., 2015). We used the Fgf17:Fgfr1 LACE assay to compare the binding of Fgf17
601 protein to HS in *WT*, *Hs2st*$^{-/-}$ and *Hs6st1*$^{-/-}$ CSB tissue at E14.5 and E16.5 in order to test the
602 hypothesis that Fgf17:HS physical interaction is selectively sensitive to loss of 2-O HS

JNeurosci Accepted Manuscript

603 sulphation in *Hs2st*$^{-/-}$ tissue (Fig 11 A-J, O). We used the Fgf8:Fgfr3 LACE assay to compare
604 the binding of Fgf8 protein to HS in *WT* and *Hs2st*$^{-/-}$ CSB tissue at E14.5 and E16.5 to test the
605 hypothesis that the Fgf8:HS physical interaction is insensitive to loss of 2-O HS sulphation in
606 *Hs2st*$^{-/-}$ tissue (Fig 11 K-N, P).

607 In both E14.5 and E16.5 *WT* tissue the Fgf17:Fgfr1 and Fgf8:Fgfr3 LACE assays
608 produced a strong LACE signal (Fig 11 A,F,K with higher magnification of boxed areas
609 enclosing CSB region shown in A', F', K'). Control experiments show this LACE signal was
610 drastically reduced by pre-treating the tissue with heparinitase to digest HS (Fig 11 D,I,M,
611 with higher magnification of CSB in D',I',M') or omitting Fgf17 or Fgf8 protein from the
612 assay (Fig 11 E,J,N with higher magnification of CSB in E',J',N'). Together these controls
613 confirm the LACE signal provides a specific readout of the interaction between each FGF
614 protein and HS molecules. To determine the effect of differential sulphation on the physical
615 interaction between HS and Fgf8 or Fgf17 we examined how the LACE signal was affected
616 when the assay was performed on *Hs2st*$^{-/-}$ and *Hs6st1*$^{-/-}$ tissue. As predicted by our hypothesis
617 the binding of Fgf17 to HS is selectively sensitive to 2-O HS sulphation as we found that the
618 Fgf17:Fgfr1 LACE signal was much weaker than *WT* in *Hs2st*$^{-/-}$ tissue (compare B,B',G,G' to
619 A,A',F,F') but similar to *WT* in *Hs6st1*$^{-/-}$ tissue (compare C,C',H,H' to A,A',F,F').
620 Quantification of Fgf17:Fgfr1 LACE signal intensity in Fig 11 O shows a significant ~4-fold
621 reduction in *Hs2st*$^{-/-}$ (green bar) compared to *WT* (blue bar) but no significant difference to
622 *WT* in *Hs6st1*$^{-/-}$ (purple bar). As predicted by our hypothesis that the binding of Fgf8 to HS is
623 not sensitive to 2-O HS sulphation we found that there was no difference in the Fgf8:Fgfr3
624 LACE signal between *WT* and *Hs2st*$^{-/-}$ tissue (compare Fig 11 K,K' to L,L'). Quantification
625 of Fgf8:Fgfr3 LACE signal intensity in Fig 11 P shows no significant difference between
626 *Hs2st*$^{-/-}$ (green bar) compared to *WT* (blue bar). These LACE results are summarised
627 schematically in Fig 11Q which shows that of the five *HST* genotype and FGF ligand
628 permutations tested only the Fgf17:HS physical interaction is sensitive to Hs2st genotype, as
629 predicted by the hypothesis that 2-O HS sulphation has a specific effect on the ability of HS
630 to bind Fgf17.

631

632 **Discussion**

633 Embryonic corpus callosum (CC) development involves multiple cell and molecular
634 events that ultimately guide callosal axons across the telencephalic midline to connect with
635 635 their synaptic targets in the contralateral hemisphere. Three subpopulations of midline
636 astroglia play pivotal roles in guiding callosal axons across the telencephalic midline. Midline

JNeurosci Accepted Manuscript

zipper (MZ) glia facilitate fusion of the cerebral hemispheres and provide a substrate for crossing callosal axons while *Slit2*$^{+}$ indusium griseum (IG) and glial wedge (GW) astroglia channel crossing axons into the correct path by Robo/Slit mediated chemorepulsion (Bagri et al., 2002; Gobius et al., 2016; Shu and Richards, 2001; Shu et al., 2003). These astroglial populations originate from RGCs born in the VZ of the septal midline and either remain in the VZ at the glial wedge (GW astroglia) or translocate in response to FGF signals, of which Fgf8 appears to be particularly important, to the pial surface of the telencephalic midline (MZ and IG astroglia) (Clegg et al., 2014; Gobius et al., 2016; Moldrich et al., 2010; Smith et al., 2006). Both Slit2^{+} IG and Slit2^{-} MZ astroglia are essential for CC development and both these astroglial populations originate from the septal VZ *Zic4* lineage so the lack of an overt CC phenotype in *Hs2st*$^{Fl/Fl}$;*Zic4*^{Cre} embryos following conditional knockout of *Hs2st* in the *Zic4* lineage indicates that neither MZ or IG astroglial precursors have a cell autonomous requirement for *Hs2st* to translocate in appropriate numbers. In *Hs2st*$^{-/-}$ embryos there is an expansion of the *Slit2* expression domain at the CSB pial surface coinciding with increased Sox9^{+} glial cells and this is phenocopied by application of exogenous Fgf17 to *Hs2st*$^{+/+}$ CSB *ex vivo* strongly suggesting increased numbers of Slit2^{+} glial cells at the midline reflect excessive GW→IG somal translocation enlarging the IG (current study). We cannot rule out the possibility that disrupted MZ glial translocation also contributes to the *Hs2st*$^{-/-}$ phenotype although this would not alter our conclusion that Hs2st plays a non-cell autonomous role in the *Zic4*-lineage astroglial translocation phenotype. Our model (Fig 10) posits that ectopic *Slit2*$^{+}$ astroglia at the midline block the transit of CC axons. In principle this could be tested by rescuing the CC axon midline crossing in *Hs2st*$^{-/-}$;*Slit2*$^{-/-}$ embryos (along similar lines to the *Slit2* genetic rescue of the *Hs6st1*$^{-/-}$ phenotype we reported in *Hs6st1*$^{-/-}$;*Slit2*$^{-/-}$ embryos (Conway et al., 2011)). However, in contrast to the fully penetrant (100%) *Hs6st1*$^{-/-}$ CC phenotype, the partial penetrance (~50%) of the *Hs2st*$^{-/-}$ CC phenotype introduces a confounding factor of distinguishing 'rescued' from 'unaffected' *Hs2st*$^{-/-}$ embryos, a problem that would be compounded if only a proportion of embryos destined to be 'affected' were rescued (see (Clegg et al., 2014; Conway et al., 2011)) so a prohibitively large number of animals would be required to demonstrate a statistically significant rescue.

Eliminating HS (*Ext1* mutagenesis) compared to 2-O HS sulphation (*Hs2st* mutagenesis) from the same cell lineages allowed us to distinguish physiological functions generally attributable to HS from those specifically requiring 2-O HS sulphation by comparing the *Ext1* and *Hs2st* phenotypes. We found that while *Zic4* lineage cells were unable to support CC development when they lacked HS (*Zic4*^{Cre};*Ext1*$^{Fl/Fl}$ embryos) there

JNeurosci Accepted Manuscript

671 was no similar requirement for 2-O HS sulphation in the *Zic4* lineage (*Zic4*^{Cre}*;Hs2st*$^{Fl/Fl}$
672 embryos) indicating that *Zic4* lineage cells require HS but that 2-O HS sulphation is
673 dispensible for their contribution to CC development, specifically the ability of astroglial
674 precursors to cell autonomously sense translocation signals. We found that HS and 2-O HS
675 sulphation are both required in the *Emx1* lineage (*Emx1*^{CreER}*;Ext1*$^{Fl/Fl}$ and
676 *Emx1*^{CreER}*;Hs2st*$^{Fl/Fl}$ embryos) although the axonal and astroglial phenotypes were not
677 identical. Somewhat counterintuitively, removing HS completely from the *Emx1* lineage in
678 *Emx1*^{CreER}*;Ext1*$^{Fl/Fl}$ embryos had a less severe effect on the distribution of GFAP^{+} midline
679 glia than preserving HS but blocking its 2-O sulphation, as the accumulation of astroglia at
680 the pial surface of the midline was much more pronounced in *Emx1*^{CreER}*;Hs2st*$^{Fl/Fl}$ embryos.
681 We speculate that completely removing HS from the *Emx1* lineage results in a general
682 destabilisation of FGF protein gradients so mitigating precocious somal translocation by *Zic4*
683 lineage astroglial precursors (Chan et al., 2017; Qu et al., 2011; Qu et al., 2012; Shimokawa
684 et al., 2011). The relatively normal midline astroglial organisation in *Emx1*^{CreER}*;Ext1*$^{Fl/Fl}$
685 embryos poses the question of whether glial disorganisation is a major contributor to their CC
686 agenesis phenotype. In *Emx1*^{CreER}*;Hs2st*$^{Fl/Fl}$ embryos the Probst bundles form right next to the
687 midline, consistent with our hypothesis that ectopic Slit2^{+} astroglia at the midline are
688 repelling CC axons from crossing the midline (Conway et al., 2011) & current study). In
689 contrast the Probst bundles in *Emx1*^{CreER}*;Ext1*$^{Fl/Fl}$ embryos form much more lateral to the
690 midline at some distance from the IG indicating CC axons are misrouted at an earlier stage of
691 their navigation than in *Emx1*^{CreER}*;Hs2st*$^{Fl/Fl}$ embryos. HS is required cell autonomously for
692 navigating axons to respond to axon guidance molecules, including Netrin1 and Slit2
693 (Matsumoto et al., 2007; Piper et al., 2006). A plausible explanation is that in
694 *Emx1*^{CreER}*;Ext1*$^{Fl/Fl}$ embryos the *Emx1* lineage HS-deficient CC axons cannot respond
695 appropriately to guidance cues that would normally guide them towards the midline and are
696 already misrouted before they come under the influence of the midline astroglia In contrast
697 *Hs2st*$^{-/-}$ CC axons express HS lacking 2-O sulphation that does not affect their ability to
698 respond to guidance cues (current study) so they reach the midline but are prevented from
699 crossing by the ectopic Slit2^{+} glia in the expanded IG.

700 Biochemical (LACE) data shows that physical interaction between Fgf17 and HS is
701 facilitated by Hs2st (but not Hs6st1) and that Hs2st facilitates physical interaction between
702 HS and Fgf17 (but not Fgf8) suggesting a molecular mechanism underpinning Hs2st
703 selectively suppressing levels of Fgf17 *in vivo* (Allen and Rapraeger, 2003; Chan et al., 2015;
704 Chan et al., 2017; Clegg et al., 2014), current study). We speculate that Hs2st exerts its

JNeurosci Accepted Manuscript

705 selective effect on Fgf17 protein levels because HS lacking 2-O HS sulphation has reduced
706 affinity for Fgf17 (but not Fgf8) so increasing the half-life of Fgf17 (but not Fgf8) in the
707 ECM by selectively reducing the rate that Fgf17 protein is cleared by HS-mediated receptor
708 mediated endocytostis of canonical FGFs while leaving Fgf8 unaffected (Yu et al., 2009).
709 Our conditional mutagenesis experiments clearly demonstrate there is no cell autonomous
710 requirement for *Hs2st* in astroglial precursor translocation in *Emx1*^{CreER}*;Hs2st*$^{Fl/Fl}$ embryos,
711 however the reduced efficiency of HS:Fgf17:Fgfr1 complex formation in the LACE assay
712 implies that *Hs2st* might also play a cell-autonomous role in the response to Fgf17 protein.
713 We speculate that even if *Hs2st*$^{-/-}$ astroglial precursors are less sensitive to Fgf17 than their
714 wild-type counterparts their translocation to the midline is primarily driven by Fgf8 so is not
715 significantly affected in *Zic4*^{Cre}*;Hs2st*$^{Fl/Fl}$ embryos. A putative reduced sensitivity of *Hs2st*$^{-/-}$
716 astroglial precursor cells to Fgf17 also begs the question of how elevated Fgf17 could trigger
717 precocious glial translocation in *Hs2st*$^{-/-}$ embryos. The Fgf17 bead assay experiment shows
718 that *Hs2st*$^{-/-}$ cells retain competence to respond to Fgf17 by phosphorylating ERK and LACE
719 data shows that HS devoid of 2-O HS sulphation still interacts with Fgf17 albeit with reduced
720 efficiency. The explanation that best fits our experimental data, therefore, is that increased
721 Fgf17 protein levels in *Hs2st*$^{-/-}$ embryos overrides any reduction in competency of *Hs2st*$^{-/-}$
722 cells to respond to Fgf17 protein and the net effect is elevated FGF/ERK signalling and
723 consequent precocious astroglial translocation.

724 This study makes two major novel contributions to our understanding of the cell and
725 molecular roles of differential HS sulphation in the regulation of forebrain development. First
726 that a primary cellular role of 2-O HS sulphation *in vivo* is not to modulate the competence of
727 astroglial precursor cells to respond to translocation signals by a cell autonomous mechanism
728 (as would be predicted by the classic role for HS in modulating the formation of the
729 FGF:FGFR:HS receptor complex on the surface of responding cells) but instead to regulate
730 the supply of translocation signals to astroglial precursors by a non cell autonomous
731 mechanism. Second that the interaction between 2-O sulphated HS and Fgf17 protein is
732 selective because it does not apply to the closely related Fgf8 protein or to 6-O HS sulphation
733 catalysed by Hs6st1. The most parsimonious explanation linking these cell and molecular
734 events is that higher than normal levels of Fgf17 protein at the CSB of *Hs2st*$^{-/-}$ embryos
735 causes the precocious astroglial precursor translocation phenotype and subsequent misrouting
736 of CC axons (Fig 10). Our rescue of the *Hs2st*$^{-/-}$ precocious astroglial precursor translocation
737 phenotype *ex vivo* by generic pharmacological inhibition of FGF signalling with SU5402
738 directly supports the hypothesis that hyperactive FGF/ERK signalling causes the phenotype.

JNeurosci Accepted Manuscript

Given the well known role of FGF/ERK signalling in triggering astroglial precursor translocation to the IG, our findings that exogenously applied Fgf17 protein is sufficient to phenocopy the *Hs2st*$^{-/-}$ astroglial precursor translocation phenotype, and that *Hs2st*$^{-/-}$ CSB cells activate ERK in response to Fgf17 protein, it is extremely unlikely that increased Fgf17 protein levels *in vivo* wouldn't result in ERK hyperactivation and consequent precocious astroglial precursor translocation in *Hs2st*$^{-/-}$ embryos. However, the current study does not provide formal proof that the elevated levels of Fgf17 protein are solely responsible for the FGF/ERK hyperactivation or precocious astroglial precursor translocation phenotypes in *Hs2st*$^{-/-}$ embryos and we were unable to design an experiment that could further discriminate between the functions of Fgf17 and Fgf8 and directly test functional selectivity of Hs2st for Fgf17 in this context. We considered employing a classic rescue experiment strategy by genetically reducing *Fgf17* dosage in *Hs2st*$^{-/-}$ embryos ('*Fgf17*$^{-/-}$*;Hs2st*$^{-/-}$' rescue) but on balance elected not to because at best it would provide equivocal evidence either for or against the hypothesis that 2-O sulphated HS interacts selectively with Fgf17 protein. FGF/ERK hyperactivation caused by overexpression of a particular FGF protein can be rescued by any experimental manipulation that restores ERK signalling to normal levels and not uniquely by restoring the levels of the FGF protein that underpins the phenotype. Specifically, reducing *Fgf17* dosage could elicit a rescue of ERK hyperactivation and collateral phenotypes at the *Hs2st*$^{-/-}$ CSB by reducing FGF/ERK signalling output whether or not abnormally high Fgf17 bioavailability was the primary cause. Analogously we interpret rescue of the *Hs6st1*$^{-/-}$ precocious astroglial precursor translocation phenotype in *Hs6st1*$^{-/-}$*;Fgf8*$^{neo/neo}$ embryos as evidence that *Hs6st1* normally acts to keep FGF/ERK signalling in check rather than as evidence for a selective genetic interaction between *Fgf8* and *Hs6st1* (Clegg et al., 2014). Conversely, failure to rescue the *Hs2st*$^{-/-}$ phenotype in *Fgf17*$^{-/-}$*;Hs2st*$^{-/-}$ embryos (or using other methods to reduce Fgf17 protein levels or functionality) would not falsify the hypothesis that increased Fgf17 bioavailability caused the *Hs2st*$^{-/-}$ phenotype because there are several alternative explanations. When we employed a similar strategy in a similar context to rescue the *Hs6st1*$^{-/-}$ astroglial precursor precocious translocation phenotype by genetically reducing *Fgf8* dosage the rescue was only successful in a minority of isogenic *Hs6st1*$^{-/-}$*;Fgf8*$^{neo/neo}$ embryos and a likely explanation is that compensatory mechanisms act when *Fgf* gene dosage is manipulated (Clegg et al., 2014). Such compensation will generate false negative results making it unsafe to interpret unrescued *Fgf17*$^{-/-}$*;Hs2st*$^{-/-}$ embryos as falsifying the hypothesis that the phenotype is underpinned by excess Fgf17 protein. There are additional technical confounds that could lead to false negatives because a rescue likely

JNeurosci Accepted Manuscript

773 requires precise restoration of normal Fgf17 protein levels (so no rescue could reflect
774 technical failure to restore Fgf17 protein levels to normal) and in any case the CC phenotype
775 of *Fgf17*$^{-/-}$ embryos has not been thoroughly characterised so *Hs2st*$^{-/-}$;*Fgf17*$^{-/-}$ phenotypes
776 may well be problematic to interpret (Cholfin and Rubenstein, 2007, 2008). In addition to not
777 being decisive for or against selectivity we note that demonstrating genetic interaction
778 between *Hs2st* and *Fgf17* would not provide insight into whether the interaction was
779 molecularly direct or not, in contrast to biochemical LACE data we present in the current
780 study.

781 The closely related '*Fgf8* subfamily' members *Fgf17* and *Fgf8* are both transcribed by
782 cells in the CSB region yet have different roles in forebrain development with available
783 evidence, while not ruling out a role for *Fgf17*, suggesting that *Fgf8* is the primary driver of
784 astroglial precursor translocation required for CC development (Cholfin and Rubenstein,
785 2007, 2008; Gobius et al., 2016; Moldrich et al., 2010; Toyoda et al., 2011). The independent
786 suppression of Fgf17 and Fgf8 protein levels by HS modified by Hs2st and Hs6st1
787 respectively may have facilitated the evolution of this system by providing a mechanism to
788 tilt the Fgf17:Fgf8 protein balance to give Fgf8 the more dominant role in regulating
789 astroglial precursor translocation (Chan et al., 2017; Clegg et al., 2014), Current study). In
790 this sense there are parallels to other negative regulatory strategies, for example micro-RNAs
791 that function by protecting cells from the expression of particular proteins that would be
792 detrimental if expressed.

793

794 **Figure Legends:**

795

796 **Figure 1.** Hs2st protein is expressed in the cerebral cortex and the septum during CC
797 formation. **(A)** Immunohistochemistry for Hs2st at E14.5 **(B-D)** Higher magnification shows
798 punctate subcellular Hs2st expression (inset, B) Hs2st protein is expressed at the CSB (B),
799 the VZ of the cortex (C) and the cortical plate (D). **(E)** Immunohistochemistry for Hs2st at
800 E18.5 **(F-M)** Hs2st protein is expressed in the IG (F), the GW (G), the septum (H), and the
801 ventral telencephalon (I). Within the cortex Hs2st is expressed at the ventricular zone (J), the
802 intermediate zone (K), Hs2st is not strongly expressed by the middle layers of the cortex (L),
803 but is expressed by the deeper layers (M). **(N-R)** Hs2st antibody specificity. The Hs2st
804 antibody produces signal in the GW (J,L), which is lost in *Hs2st*$^{-/-}$ embryos (K,M). Western-
805 blot performed on protein extracted from whole telencephalon using Hs2st antibody reveals
806 the predicted ~42kDa band in WT extracts, which is lost in *Hs2st*$^{-/-}$ extracts (N). B-D are

JNeurosci Accepted Manuscript

807 higher magnification images of boxed regions indicated in A. F-M are higher magnification
808 images of boxed regions indicated in E. L and M are higher magnification images of boxed
809 regions in J and K respectively. Insets in B, F, P and Q are higher magnification images of
810 boxed regions. Scale bars: 500µm in A, 50µm in B-I, L, M; 100µm in J,K.

811

812 **Figure 2**. *Slit2* expression at the CSB of WT and *Hs2st*$^{-/-}$ embryos at E16.5. **(A, C, E)** *In-situ*
813 hybridisation for *Slit2* in WT embryos at 3 rostro-caudal positions labelling the GW and IG.
814 **(B, D, F)** *In situ* hybridisation for *Slit2* in *Hs2st*$^{-/-}$ embryos at equivalent positions to A, C and
815 E respectively showing an expanded IG. Scale bar: 100µm in all panels.

816

817 **Figure 3.** *Emx1* and *Zic4* lineage contribution at the CSB. **(A)** *Zic4*^{cre} allele combined with a
818 lox-stop GFP reporter has been used to label cell populations at E18.5. *Zic4*^{cre} labels cells of
819 the septum. **(B, C, D, E)** *Zic4*^{cre} labels cells ventral to the CSB (dashed line, B,C) including
820 *Sox9* expressing cells (arrowheads, C) but is not expressed by *Sox9* expressing cells dorsal to
821 the CSB (arrows, C). *Zic4*^{cre} is expressed by IG glial cells (arrowheads, D) but not by
822 surrounding cells. *Zic4*^{cre} is expressed by MZ glial cells (arrowheads, E). **(F)** Schematic of
823 the *Zic4*^{cre} expressing cell lineage. **(G)** *Emx1*^{creER} allele combined with a lox-stop GFP
824 reporter has been used to label cell populations at E18.5. *Emx1*^{creER} labels cells of the cortex.
825 **(H, I, J, K)** *Emx1*^{creER} labels cells dorsal to the CSB (dashed line, H,I) including *Sox9*
826 expressing cells (arrowheads, I) but is not expressed by *Sox9* expressing cells ventral to the
827 CSB (arrows, I). *Emx1*^{creER} is not expressed by IG glial cells (arrows, J). *Emx1*^{creER} is not
828 expressed by MZ glial cells (arrows, K). **(L)** Schematic of the *Emx1* expressing cell lineage.
829 No phenotype was detected in *Hs2st*$^{+/+}$ *Zic4*^{cre} or *Hs2st*$^{+/+}$ *Emx1*^{creER} embryos (n=5 for each
830 genotype). C, D and E are higher magnification images of the indicated regions in B. I, J and
831 K are higher magnification images of the indicated regions in H. Scale bars: 500µm in A,G;
832 200µm in B and H; 50µm in C-E and I-K.

833

834 **Figure 4.** HS expression is required within both *Emx1* and *Zic4* lineage cells for CC
835 formation. **(A-I)** Immunofluorescence for L1 (red) at E18.5 labels the CC while GFAP
836 (green) labels glia. In control embryos the U-shaped CC has formed and is flanked by glia at
837 the IG and GW (A, D, G). In *Ext1*$^{fl/fl}$ *Emx1*^{creER} embryos CC axons do not cross the midline
838 while glia at the IG and GW appear largely unaffected (B, E, H). In *Ext1*$^{fl/fl}$ *Zic4*^{cre} embryos
839 CC axon do not cross the midline while glia appear depleted at the IG and form abnormal
840 bundles at the GW (C, F, I). **(J-O)** FGFR1/ FGF2 ligand and carbohydrate engagement

JNeurosci Accepted Manuscript

841 (LACE) assay is used to detect the presence of HS. In control embryos LACE signal can be
842 seen throughout the telencephalon, and is of similar intensity within both the cortex and the
843 septum (J, M). In *Ext1*$^{fl/fl}$ *Emx1*^{creER} embryos LACE signal is significantly reduced within the
844 cortex (K, N). In *Ext1*$^{fl/fl}$ *Zic4*^{cre} embryos LACE signal is significantly reduced within the
845 septum (L, O). D-I are higher magnification images of the indicated boxed regions in A-C, J-
846 L are higher magnification images of the boxed region in G-I respectively. Scale Bars:
847 200µm in A-C and G-I; 100µm in D-F and J-L.
848
849 **Figure 5.** *Hs2st* expression is required within *Emx1* lineage cells but not *Zic4* lineage cells
850 for CC formation. **(A-C)** Immunofluorescence for L1 and GFAP at E18.5. In control embryos
851 the U-shaped CC has formed and the IG can be observed above the CC (A). In *Hs2st*$^{fl/fl}$
852 *Zic4*^{cre} embryos the CC and IG form normally (B). In around half of *Hs2st*$^{fl/fl}$;*Emx1*^{creER}
853 embryos the CC fails to form, IG glia also extend ventrally (asterisks, C). In the remaining
854 *Hs2st*$^{fl/fl}$;*Emx1*^{creER} embryos the CC forms normally (C'). **(D-I)** Immunofluorescence for *Sox9*
855 labels progenitor cells at the ventricular zone and mature glia at the IG, GFP labels cells in
856 which cre is active. (D, G) In control (*Hs2st*$^{+/+}$;*Emx1*^{creER}) embryos IG glia do not express
857 GFP. (E, H) In *Hs2st*$^{fl/fl}$;*Zic4*^{cre} embryos IG glia do express GFP and adopt their normal
858 position. (F, I) In *Hs2st*$^{fl/fl}$;*Emx1*^{creER} embryos GFP is expressed by cortical neurons and
859 axons but not by abnormally positioned IG glia. **(J-L)** Immunohistochemistry for Hs2st
860 shows expression of Hs2st in the IG. (J) in control embryos punctate Hs2st staining can be
861 seen within IG cells. In *Hs2st*$^{fl/fl}$ *Zic4*^{cre} embryos Hs2st is not expressed by IG glia (K). In
862 *Hs2st*$^{fl/fl}$;*Emx1*^{creER} embryos Hs2st is expressed by displaced glial cells (L). Hs2st
863 immunohistochemistry in J-L was performed on adjacent tissue sections to those in D-I. **(M)**
864 Quantification of Sox9 expressing cell number at the IG in control (blue bar, n=4 embryos, *2*
865 *Hs2st*$^{+/+}$;*Zic4*^{cre}+ *2 Hs2st*$^{+/+}$;*Emx1*^{creER}), affected *Hs2st*$^{fl/fl}$;*Emx1*^{creER} (orange bar, n=4
866 embryos), and *Hs2st*$^{fl/fl}$;*Zic4*^{cre} (purple bar, n=3 embryos). Sox9^{+} numbers are significantly
867 increased compared to control in *Hs2st*$^{fl/fl}$;*Emx1*^{creER} embryos (* indicates $p<0.05$ on graph),
868 ($F(2, 7) = 42.16$, $p = 0.00013$, ANOVA), post-hoc t-tests: control vs *Hs2st*$^{fl/fl}$;*Emx1*^{creER} ($t(4)$
869 $= -8.08$, $p = 0.0013$, t-test); & control vs *Hs2st*$^{fl/fl}$;*Zic4*^{cre} ($t(5) = 0.92$, $p = 0.40$, t-test). Boxed
870 regions in G-I are higher magnification images of boxed regions in D-F respectively. Insets in
871 J, K and L are higher magnification images of boxed region shown on each image. Scale
872 bars: 200µm in A-F; 100µm 50µm in G-I and J-L.
873

JNeurosci Accepted Manuscript

874 **Figure 6**: *Hs2st* is not required by CC axons in order to cross the telencephalic midline. **(A,**
875 **D)** After homotypic transplantation of E17.5 cortical explants from GFP^+ control tissue into
876 the cortex of GFP^- control brain slices GFP^+ CC axons are able to project across the midline
877 (arrows, D). **(B, E)** After transplantation of GFP^+ $Hs2st^{-/-}$ cortical explants into GFP^- control
878 brain slices GFP^+ CC axons are able to project across the midline (arrows, E). **(C, F)** After
879 transplantation of cortical explants from GFP^+ control tissue into the cortex of GFP^- $Hs2st^{-/-}$
880 brain slices GFP^+ CC axons are unable to project across the midline and invade the septum.
881 Arrowheads indicate axons navigating into the septum in all conditions. **(G-I)** Schematic of
882 transplant experiments shown in A-C. D-F are higher magnification images of the boxed
883 region in A-C respectively. Scale bars: 200µm in all panels.
884

885 **Figure 7.** Hyperactive Fgf signalling causes precocious glia translocation in $Hs2st^{-/-}$ CSB.
886 **(A)** Experimental outline of $Hs2st^{-/-}$ phenotypic rescue experiment. Pregnant females were
887 injected at E14.5 with a BrdU pulse and CSB slices collected after 1 hour and cultured for
888 48hrs **(B-I)** *WT* or $Hs2st^{-/-}$ CSB slices were cultured in the presence of either SU5402 (FGFi)
889 or DMSO (untreated vehicle control). (B, D, F, H) pErk immunohistochemistry shows that
890 FGFi treatment reduces Fgf/ERK signalling. (C,E,G,I) Immunofluorescence for BrdU and
891 Sox9 in *WT* (C,E) and $Hs2st^{-/-}$ (G,I) slices treated with FGFi (E,I) or untreated (C,G), the
892 curved dotted line demarcates the basal edge of the VZ, arrows in C,G point to accumulations
893 of $BrdU/Sox9^+$ cells at the midline (arrow size corresponds to cell number) with higher
894 magnification insets showing $Sox9/BrdU^+$ (yellow) double labelled cells in IG region. (J)
895 Quantification of $Sox9/BrdU^+$ double labelled cells in *WT* or $Hs2st^{-/-}$ CSB slice cultures
896 treated with FGFi or untreated (n=3 embryos for each condition). For both genotypes FGFi
897 treatment significantly reduces the number of $Sox9/BrdU^+$ cells that exit the VZ and moved
898 towards the IG at one or more rostro-caudal position (significant differences due to FGFi
899 treatment within each genotype indicated on graph as **$p<0.05$ ***$p<0.001$). ($F(3, 32) =$
900 31.00, $p = 0.0000000014$, Two-way ANOVA) followed by t-test with Sidak's correction for
901 multiple comparisons at each positon along the rostro-caudal axis. *WT* FGFi vs *WT* untreated:
902 position 1 ($t(16) = 1.67$, $p = 0.24$, t-test); position 2 ($t(16) = 2.37$, $p = 0.11$, t-test); position 3
903 ($t(16) = 2.25$, $p = 0.15$, t-test); & position 4 ($t(16) = 2.81$, $p = 0.050$, t-test). $Hs2st^{-/-}$ FGFi vs
904 $Hs2st^{-/-}$ untreated: position 1 ($t(16) = 2.38$, $p = 0.11$, t-test); position 2 ($t(16) = 2.83$, $p =$
905 0.048, t-test); position 3 ($t(16) = 3.05$, $p = 0.030$, t-test); & position 4 ($t(16) = 4.60$, $p =$
906 0.0012, t-test). Scale bars: 100µm B-I.

JNeurosci Accepted Manuscript

907 **Figure 8**. Expression of Fgf17 during CSB development in *WT* and *Hs2st*$^{-/-}$ and *Hs6st1*$^{-/-}$
908 embryos. **(A-C)** Fgf17 protein and mRNA expression at the E12.5 CSB of *WT* and *Hs2st*$^{-/-}$
909 embryos. Fgf17 protein is expressed across the CSB in both *WT* and *Hs2st*$^{-/-}$ embryos, with
910 no obvious change in intensity or domain of expression. *Fgf17* mRNA expression overlaps
911 well with the protein expression domain and is similar between *WT* and *Hs2st*$^{-/-}$. **(D-F)** Fgf17
912 protein and mRNA expression at the E14.5 CSB of *WT* and *Hs2st*$^{-/-}$ embryos. Fgf17 protein is
913 expressed at low levels at the CSB of *WT* embryos. In *Hs2st*$^{-/-}$ embryos, the protein
914 expression domain expands across the CSB (asterisks in E_2). *Fgf17* mRNA is unchanged at
915 the CSB between *WT* and *Hs2st*$^{-/-}$ embryos. **(G-I)** Fgf17 protein and mRNA expression at the
916 E16.5 CSB of *WT* and *Hs2st*$^{-/-}$ embryos. Fgf17 protein is expressed at low levels at the CSB
917 of *WT* embryos (H_1). In *Hs2st*$^{-/-}$ embryos, the protein expression domain expands (asterisks,
918 H_2). There is a concurrent increase in *Fgf17* mRNA (asterisk, I_2). **(J-O)** Fgf17 mRNA (J,
919 $K_{1,2,3}$ $L_{1,2,3}$) and Fgf17 protein (M, $N_{1,2,3}$ $O_{1,2,3}$) expression (red) relative to GFP$^+$ *Zic4* lineage
920 cells (indicated with white arrows) at the GW ($K_{1,2,3}$, $N_{1,2,3}$) and IG ($L_{1,2,3}$, $O_{1,2,3}$) of *WT* E14.5
921 embryos. **(P)** E14.5 expression of Hs2st by LacZ staining. Hs2st is expressed most highly at
922 the VZ, with decreasing expression towards the pial surface. **(Q-V)** Fgf17 protein and mRNA
923 expression at the E14.5 CSB of *WT* and *Hs6st1*$^{-/-}$ embryos. Fgf17 protein is expressed at low
924 levels at the CSB of WT embryos (Q_1,R_1). In *Hs6st1*$^{-/-}$ embryos, the protein expression
925 domain is similar to WT (Q_2,R_2). *Fgf17* mRNA expression is unchanged between *WT* and
926 *Hs6st1*$^{-/-}$ embryos (S_1, S_2). **(T-V)** Fgf17 protein and mRNA expression at the E16.5 CSB of
927 *WT* and *Hs6st1*$^{-/-}$ embryos. Fgf17 protein is expressed at very low levels at the CSB of both
928 *WT* (T_1, U_1) and *Hs6st1*$^{-/-}$ (T_2, U_2) embryos. *Fgf17* mRNA expression is unchanged between
929 *WT* (V_1) and *Hs6st1*$^{-/-}$ (V_2) embryos. **(W)** Quantification of Fgf17 immunofluorescence signal
930 at CSB in *WT* (blue bar, n=3 embryos), *Hs2st*$^{-/-}$ (green bar, n=3 embryos) and *Hs6st1*$^{-/-}$
931 (purple bar, n=3 embryos). Fgf17 protein level is significantly increased compared to *WT* in
932 *Hs2st*$^{-/-}$ embryos (* indicates $p<0.05$ on graph), ($F(2, 9) = 13.83$, $p = 0.0018$, ANOVA), post-
933 hoc t-tests: *WT* vs *Hs2st*$^{-/-}$ ($t(4) = -4.22$, $p = 0.014$, t-test); & *WT* vs *Hs6st1*$^{-/-}$ ($t(6) = -0.98$, p
934 $= 0.36$, t-test). Boxed areas in A,D,G,Q,T shown at higher magnification in B,E,H,R,U
935 respectively. Scale bars: 200µm in A,D,G,Q,T; 100µm in B,C,E,F,H,I,R,S,U,V,J,M,P; 10µm
936 in K,L,N,O.

937

938

JNeurosci Accepted Manuscript

939 **Figure 9.** Fgf17-bead experiment. **(A)** Experimental outline of Fgf17 protein bead
940 experiment in WT embryos. Pregnant females were injected at E14.5 with a BrdU pulse and
941 CSB slices collected. One Fgf17 and one BSA bead were added to each side of the midline.
942 **(B)** Fgf17 protein and pErk after 2 hours in culture. In both *WT* and *Hs2st*$^{-/-}$ CSB slices, Fgf17
943 and pErk are seen in tissue surrounding the Fgf17 bead. Staining for either is absent around
944 the BSA bead (demarcated by dotted circle). **(C)** Immunofluorescence for BrdU and Sox9
945 was performed on slices after 48 hours in culture, curved dotted lines indicate the basal edge
946 of the VZ and straight dotted line indicates the midline. D shows a higher power of the
947 arrowed regions in C. **(E)** Quantification of Sox9^{+}/BrdU^{+} double labelled cells in CSB slice
948 cultures with Fgf17 or BSA bead. The Fgf17 bead significantly increased the number of
949 Sox9^{+}/BrdU^{+} cells that exit the VZ and moved towards the IG (significant differences
950 indicated on graph as **$p<0.05$ ***$p<0.001$) at the four caudal-most positions (n=5
951 embryos). ($F(1, 48) = 65.63$, $p = 0.000000000155$, Two-way ANOVA) followed by t-test
952 with Sidak's correction for multiple comparisons for Fgf17-bead vs BSA-bead at each
953 rostral-caudal position: position 1 ($t(48) = 1.45$, $p = 0.63$, t-test); position 2 ($t(48) = 2.36$, $p =$
954 0.13, t-test); position 3 ($t(48) = 3.65$, $p = 0.0039$, t-test); position 4 ($t(48) = 4.47$, $p = 0.0003$,
955 t-test); position 5 ($t(48) = 4.03$, $p = 0.0012$, t-test); & position 6 ($t(48) = 3.89$, $p = 0.0018$, t-
956 test). **(F)** *Slit2* expression in slices cultured with Fgf17 and BSA beads. Scale bars: 100µm.

957

958 **Figure 10** Model. Hs2st expressed in *Emx1* lineage cells catalyses 2-O HS sulphation (2-O
959 HS) that in turn supresses levels of Fgf17 protein, but not Fgf8 protein, by an unknown
960 mechanism at the CSB. *Zic4* lineage astroglial precursors respond to Fgf8 and Fgf17 protein
961 by activating FGF/ERK signalling and translocating (black arrows) to the midline. This
962 generates appropriate positioning of *Slit2*$^{+}$ astroglia to guide corpus callosum axons across
963 the midline. Loss of 2-O HS from the *Emx1* lineage selectively de-supresses Fgf17 protein
964 levels while leaving Fgf8 protein unaffected. This causes hyperactive FGF/ERK signalling
965 and more *Zic4* lineage astroglial precursors translocate than normal with consequent blocking
966 of corpus callosum axon midline crossing by the ectopic midline *Slit2*$^{+}$ astroglia. *Zic4* lineage
967 astroglial precursor cells do not need to express 2-O HS in order to respond to FGF signalling
968 proteins and translocate to the midline.

969

JNeurosci Accepted Manuscript

Figure 11 Ligand and carbohydrate engagement (LACE) assay for FGF:HS interactions**. (A-J, O)** FGFR1/FGF17 LACE experiments on **(A-E)** E14.5 and **(F-J)** E16.5 telencephalic coronal sections through the CSB. **(A,F)** *WT*, **(B,G)** *Hs2st*$^{-/-}$, **(C,H)** *Hs6st1*$^{-/-}$ **(D,I)** WT sections pretreated with Heparinitase to digest HS, **(E,J)** WT sections with FGF17 ommitted from the LACE assay. (**O**) Quantification of FGF17/FGFR1 LACE signal in *WT* (blue bar, n=9 embryos), *Hs2st*$^{-/-}$ (green bar, n=5 embryos), and *Hs6st1*$^{-/-}$ (purple bar, n=4 embryos), showing a significant decrease (* indicates $p<0.05$ on graph) in *Hs2st*$^{-/-}$ embryos,($F(2, 15) = 8.62$, $p = 0.0032$, ANOVA), followed by post-hoc t test: *WT* vs *Hs2st*$^{-/-}$ ($t(9) = 6.11$, $p = 0.014$, t-test); & *WT* vs *Hs6st1*$^{-/-}$ ($t(5) = 0.63$, $p = 0.56$, t-test) (**K-N, P**) FGFR3/FGF8 LACE experiments on E14.5 telencephalic coronal sections through the CSB. (**K**) *WT*, (**L**) *Hs2st*$^{-/-}$, (**M**) WT sections pretreated with Heparinitase to digest HS, (**N**) WT sections with FGF8 ommitted from the LACE assay. (**P**) Quantification of FGF8/FGFR3 LACE signal in *WT* (blue bar, n=3 embryos), *Hs2st*$^{-/-}$ (green bar, n=3 embryos) shows no significant difference ($t(3) = 0.29$, $p = 0.76$, t-test). Numbers of embryos of each genotype analysed indicated under bars. (**Q**) Summary diagram. FGFR1/FGF17/HS complex formation is equally supported by *WT* and *Hs6st1*$^{-/-}$ HS but less so by *Hs2st*$^{-/-}$ HS while FGFR3/FGF8/HS complex formation is equally supported by *WT* and *Hs2st*$^{-/-}$ HS showing that FGF17:HS physical molecular interaction is selectively dependent on 2-O HS sulphation. Higher magnification showing the CSB region boxed in A-N are shown in A'-N' (note the DAPI channel is not shown in the higher magnification images to improve visualisation of the LACE signal). Scale bars 200µm.

References

Allen, B.L., Filla, M.S., Rapraeger, A.C., 2001. Role of heparan sulfate as a tissue-specific regulator of FGF-4 and FGF receptor recognition. J Cell Biol 155, 845-858.

Allen, B.L., Rapraeger, A.C., 2003. Spatial and temporal expression of heparan sulfate in mouse development regulates FGF and FGF receptor assembly. J Cell Biol 163, 637-648.

Bagri, A., Marin, O., Plump, A.S., Mak, J., Pleasure, S.J., Rubenstein, J.L., Tessier-Lavigne, M., 2002. Slit proteins prevent midline crossing and determine the dorsoventral position of major axonal pathways in the mammalian forebrain. Neuron 33, 233-248.

Balasubramanian, R., Zhang, X., 2016. Mechanisms of FGF gradient formation during embryogenesis. Semin Cell Dev Biol 53, 94-100.

JNeurosci Accepted Manuscript

1002 Belenkaya, T.Y., Han, C., Yan, D., Opoka, R.J., Khodoun, M., Liu, H., Lin, X., 2004.
1003 Drosophila Dpp morphogen movement is independent of dynamin-mediated endocytosis but
1004 regulated by the glypican members of heparan sulfate proteoglycans. Cell 119, 231-244.
1005 Bullock, S.L., Fletcher, J.M., Beddington, R.S., Wilson, V.A., 1998. Renal agenesis in mice
1006 homozygous for a gene trap mutation in the gene encoding heparan sulfate 2-sulfotransferase.
1007 Genes Dev 12, 1894-1906.
1008 Chan, W.K., Howe, K., Clegg, J.M., Guimond, S.E., Price, D.J., Turnbull, J.E., Pratt, T.,
1009 2015. 2-O Heparan Sulfate Sulfation by Hs2st Is Required for Erk/Mapk Signalling
1010 Activation at the Mid-Gestational Mouse Telencephalic Midline. PLoS One 10, e0130147.
1011 Chan, W.K., Price, D.J., Pratt, T., 2017. FGF8 morphogen gradients are differentially
1012 regulated by heparan sulphotransferases Hs2st and Hs6st1 in the developing brain. Biol Open
1013 6, 1933-1942.
1014 Cholfin, J.A., Rubenstein, J.L., 2007. Patterning of frontal cortex subdivisions by Fgf17. Proc
1015 Natl Acad Sci U S A 104, 7652-7657.
1016 Cholfin, J.A., Rubenstein, J.L., 2008. Frontal cortex subdivision patterning is coordinately
1017 regulated by Fgf8, Fgf17, and Emx2. J Comp Neurol 509, 144-155.
1018 Christian, J.L., 2012. Morphogen gradients in development: from form to function. Wiley
1019 Interdiscip Rev Dev Biol 1, 3-15.
1020 Clegg, J.M., Conway, C.D., Howe, K.M., Price, D.J., Mason, J.O., Turnbull, J.E., Basson,
1021 M.A., Pratt, T., 2014. Heparan sulfotransferases hs6st1 and hs2st keep erk in check for mouse
1022 corpus callosum development. J Neurosci 34, 2389-2401.
1023 Conway, C.D., Howe, K.M., Nettleton, N.K., Price, D.J., Mason, J.O., Pratt, T., 2011.
1024 Heparan sulfate sugar modifications mediate the functions of slits and other factors needed
1025 for mouse forebrain commissure development. J Neurosci 31, 1955-1970.
1026 Donahoo, A.L., Richards, L.J., 2009. Understanding the mechanisms of callosal development
1027 through the use of transgenic mouse models. Semin Pediatr Neurol 16, 127-142.
1028 Erskine, L., Williams, S.E., Brose, K., Kidd, T., Rachel, R.A., Goodman, C.S., Tessier-
1029 Lavigne, M., Mason, C.A., 2000. Retinal ganglion cell axon guidance in the mouse optic
1030 chiasm: expression and function of robos and slits. J Neurosci 20, 4975-4982.
1031 Gobius, I., Morcom, L., Suarez, R., Bunt, J., Bukshpun, P., Reardon, W., Dobyns, W.B.,
1032 Rubenstein, J.L., Barkovich, A.J., Sherr, E.H., Richards, L.J., 2016. Astroglial-Mediated
1033 Remodeling of the Interhemispheric Midline Is Required for the Formation of the Corpus
1034 Callosum. Cell Rep 17, 735-747.

JNeurosci Accepted Manuscript

1035 Guillemot, F., Zimmer, C., 2011. From cradle to grave: the multiple roles of fibroblast
1036 growth factors in neural development. Neuron 71, 574-588.
1037 Hoch, R.V., Clarke, J.A., Rubenstein, J.L., 2015. Fgf signaling controls the telencephalic
1038 distribution of Fgf-expressing progenitors generated in the rostral patterning center. Neural
1039 Dev 10, 8.
1040 Inatani, M., Irie, F., Plump, A.S., Tessier-Lavigne, M., Yamaguchi, Y., 2003. Mammalian
1041 brain morphogenesis and midline axon guidance require heparan sulfate. Science 302, 1044-
1042 1046.
1043 Kessaris, N., Fogarty, M., Iannarelli, P., Grist, M., Wegner, M., Richardson, W.D., 2006.
1044 Competing waves of oligodendrocytes in the forebrain and postnatal elimination of an
1045 embryonic lineage. Nat Neurosci 9, 173-179.
1046 Kinnunen, T., Huang, Z., Townsend, J., Gatdula, M.M., Brown, J.R., Esko, J.D., Turnbull,
1047 J.E., 2005. Heparan 2-O-sulfotransferase, hst-2, is essential for normal cell migration in
1048 Caenorhabditis elegans. Proc Natl Acad Sci U S A 102, 1507-1512.
1049 Kreuger, J., Spillmann, D., Li, J.P., Lindahl, U., 2006. Interactions between heparan sulfate
1050 and proteins: the concept of specificity. J Cell Biol 174, 323-327.
1051 Li, J.P., Kusche-Gullberg, M., 2016. Heparan Sulfate: Biosynthesis, Structure, and Function.
1052 Int Rev Cell Mol Biol 325, 215-273.
1053 Loo, B.M., Kreuger, J., Jalkanen, M., Lindahl, U., Salmivirta, M., 2001. Binding of
1054 heparin/heparan sulfate to fibroblast growth factor receptor 4. J Biol Chem 276, 16868-
1055 16876.
1056 Loo, B.M., Salmivirta, M., 2002. Heparin/Heparan sulfate domains in binding and signaling
1057 of fibroblast growth factor 8b. J Biol Chem 277, 32616-32623.
1058 Makarenkova, H.P., Hoffman, M.P., Beenken, A., Eliseenkova, A.V., Meech, R., Tsau, C.,
1059 Patel, V.N., Lang, R.A., Mohammadi, M., 2009. Differential interactions of FGFs with
1060 heparan sulfate control gradient formation and branching morphogenesis. Sci Signal 2, ra55.
1061 Matsumoto, Y., Irie, F., Inatani, M., Tessier-Lavigne, M., Yamaguchi, Y., 2007. Netrin-
1062 1/DCC signaling in commissural axon guidance requires cell-autonomous expression of
1063 heparan sulfate. J Neurosci 27, 4342-4350.
1064 Moldrich, R.X., Gobius, I., Pollak, T., Zhang, J., Ren, T., Brown, L., Mori, S., De Juan
1065 Romero, C., Britanova, O., Tarabykin, V., Richards, L.J., 2010. Molecular regulation of the
1066 developing commissural plate. J Comp Neurol 518, 3645-3661.

JNeurosci Accepted Manuscript

1067 Niquille, M., Garel, S., Mann, F., Hornung, J.P., Otsmane, B., Chevalley, S., Parras, C.,
1068 Guillemot, F., Gaspar, P., Yanagawa, Y., Lebrand, C., 2009. Transient neuronal populations
1069 are required to guide callosal axons: a role for semaphorin 3C. PLoS Biol 7, e1000230.
1070 Ornitz, D.M., Itoh, N., 2015. The Fibroblast Growth Factor signaling pathway. Wiley
1071 Interdiscip Rev Dev Biol 4, 215-266.
1072 Piper, M., Anderson, R., Dwivedy, A., Weinl, C., van Horck, F., Leung, K.M., Cogill, E.,
1073 Holt, C., 2006. Signaling mechanisms underlying Slit2-induced collapse of Xenopus retinal
1074 growth cones. Neuron 49, 215-228.
1075 Pratt, T., Conway, C.D., Tian, N.M., Price, D.J., Mason, J.O., 2006. Heparan sulphation
1076 patterns generated by specific heparan sulfotransferase enzymes direct distinct aspects of
1077 retinal axon guidance at the optic chiasm. J Neurosci 26, 6911-6923.
1078 Pratt, T., Sharp, L., Nichols, J., Price, D.J., Mason, J.O., 2000. Embryonic stem cells and
1079 transgenic mice ubiquitously expressing a tau-tagged green fluorescent protein. Dev Biol
1080 228, 19-28.
1081 Qu, X., Carbe, C., Tao, C., Powers, A., Lawrence, R., van Kuppevelt, T.H., Cardoso, W.V.,
1082 Grobe, K., Esko, J.D., Zhang, X., 2011. Lacrimal gland development and Fgf10-Fgfr2b
1083 signaling are controlled by 2-O- and 6-O-sulfated heparan sulfate. J Biol Chem 286, 14435-
1084 14444.
1085 Qu, X., Pan, Y., Carbe, C., Powers, A., Grobe, K., Zhang, X., 2012. Glycosaminoglycan-
1086 dependent restriction of FGF diffusion is necessary for lacrimal gland development.
1087 Development 139, 2730-2739.
1088 Ramsbottom, S.A., Maguire, R.J., Fellgett, S.W., Pownall, M.E., 2014. Sulf1 influences the
1089 Shh morphogen gradient during the dorsal ventral patterning of the neural tube in Xenopus
1090 tropicalis. Dev Biol 391, 207-218.
1091 Rubin, A.N., Alfonsi, F., Humphreys, M.P., Choi, C.K., Rocha, S.F., Kessaris, N., 2010. The
1092 germinal zones of the basal ganglia but not the septum generate GABAergic interneurons for
1093 the cortex. J Neurosci 30, 12050-12062.
1094 Shimokawa, K., Kimura-Yoshida, C., Nagai, N., Mukai, K., Matsubara, K., Watanabe, H.,
1095 Matsuda, Y., Mochida, K., Matsuo, I., 2011. Cell surface heparan sulfate chains regulate
1096 local reception of FGF signaling in the mouse embryo. Dev Cell 21, 257-272.
1097 Shu, T., Richards, L.J., 2001. Cortical axon guidance by the glial wedge during the
1098 development of the corpus callosum. J Neurosci 21, 2749-2758.
1099 Shu, T., Sundaresan, V., McCarthy, M.M., Richards, L.J., 2003. Slit2 guides both precrossing
1100 and postcrossing callosal axons at the midline in vivo. J Neurosci 23, 8176-8184.

JNeurosci Accepted Manuscript

1101 Smith, K.M., Ohkubo, Y., Maragnoli, M.E., Rasin, M.R., Schwartz, M.L., Sestan, N.,
1102 Vaccarino, F.M., 2006. Midline radial glia translocation and corpus callosum formation
1103 require FGF signaling. Nat Neurosci 9, 787-797.
1104 Sousa, V.H., Miyoshi, G., Hjerling-Leffler, J., Karayannis, T., Fishell, G., 2009.
1105 Characterization of Nkx6-2-derived neocortical interneuron lineages. Cereb Cortex 19 Suppl
1106 1, i1-10.
1107 Stanford, K.I., Wang, L., Castagnola, J., Song, D., Bishop, J.R., Brown, J.R., Lawrence, R.,
1108 Bai, X., Habuchi, H., Tanaka, M., Cardoso, W.V., Kimata, K., Esko, J.D., Heparan sulfate 2-
1109 O-sulfotransferase is required for triglyceride-rich lipoprotein clearance. J Biol Chem 285,
1110 286-294.
1111 Toyoda, R., Assimacopoulos, S., Wilcoxon, J., Taylor, A., Feldman, P., Suzuki-Hirano, A.,
1112 Shimogori, T., Grove, E.A., 2011. FGF8 acts as a classic diffusible morphogen to pattern the
1113 neocortex. Development 137, 3439-3448.
1114 Turnbull, J., Powell, A., Guimond, S., 2001. Heparan sulfate: decoding a dynamic
1115 multifunctional cell regulator. Trends Cell Biol 11, 75-82.
1116 Wallace, V.A., Raff, M.C., 1999. A role for Sonic hedgehog in axon-to-astrocyte signalling
1117 in the rodent optic nerve. Development 126, 2901-2909.
1118 Wang, Y., Kim, E., Wang, X., Novitch, B.G., Yoshikawa, K., Chang, L.S., Zhu, Y., 2012.
1119 ERK inhibition rescues defects in fate specification of Nf1-deficient neural progenitors and
1120 brain abnormalities. Cell 150, 816-830.
1121 Xu, J., Lawshe, A., MacArthur, C.A., Ornitz, D.M., 1999. Genomic structure, mapping,
1122 activity and expression of fibroblast growth factor 17. Mech Dev 83, 165-178.
1123 Yan, D., Lin, X., 2009. Shaping morphogen gradients by proteoglycans. Cold Spring Harb
1124 Perspect Biol 1, a002493.
1125 Yu, S.R., Burkhardt, M., Nowak, M., Ries, J., Petrasek, Z., Scholpp, S., Schwille, P., Brand,
1126 M., 2009. Fgf8 morphogen gradient forms by a source-sink mechanism with freely diffusing
1127 molecules. Nature 461, 533-536.
1128 Zhang, H., Newman, D.R., Sannes, P.L., 2012a. HSULF-1 inhibits ERK and AKT signaling
1129 and decreases cell viability in vitro in human lung epithelial cells. Respir Res 13, 69.
1130 Zhang, X., Bao, L., Yang, L., Wu, Q., Li, S., 2012b. Roles of intracellular fibroblast growth
1131 factors in neural development and functions. Sci China Life Sci 55, 1038-1044.

1132

JNeurosci Accepted Manuscript

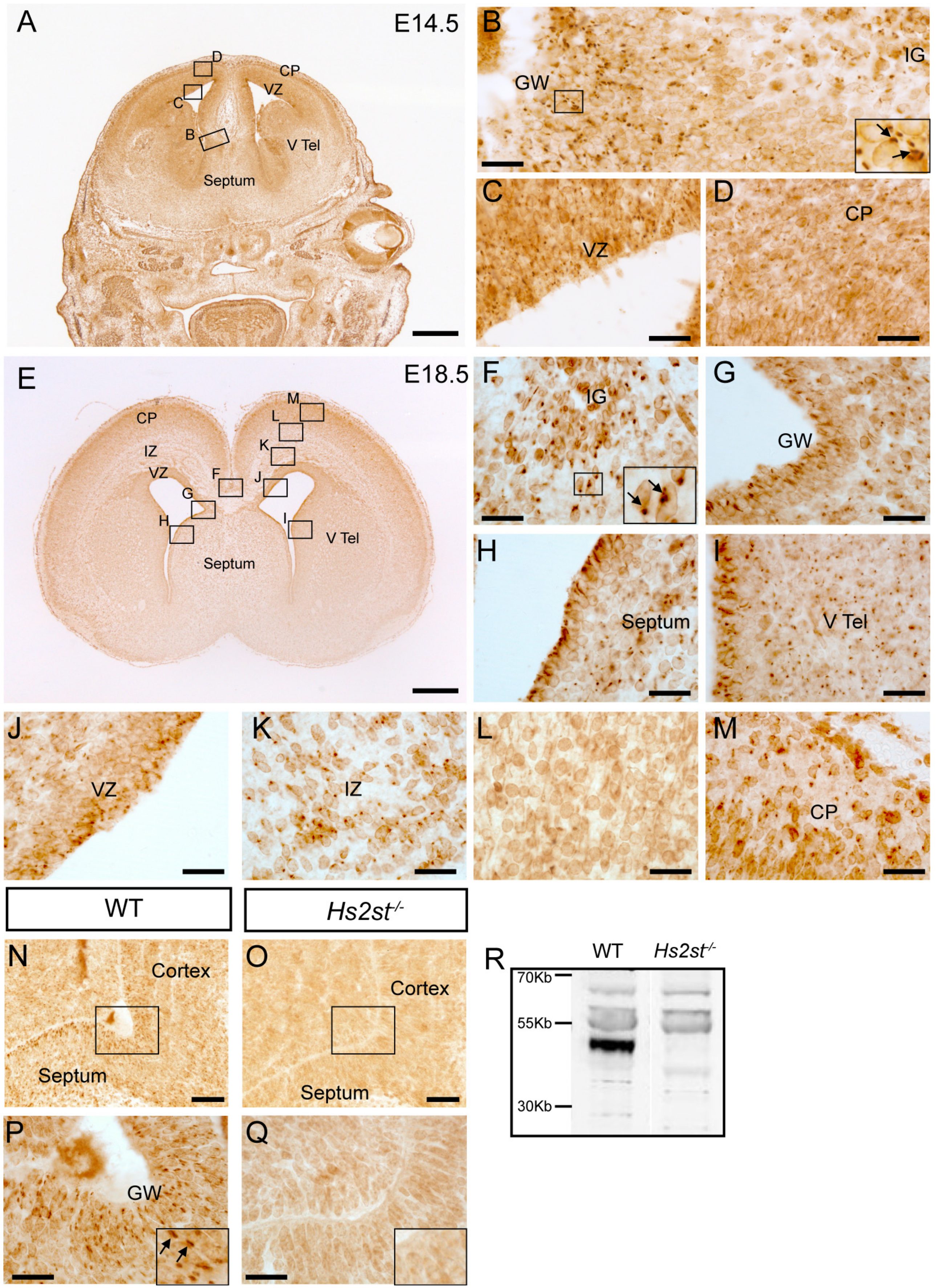

JNeurosci Accepted Manuscript

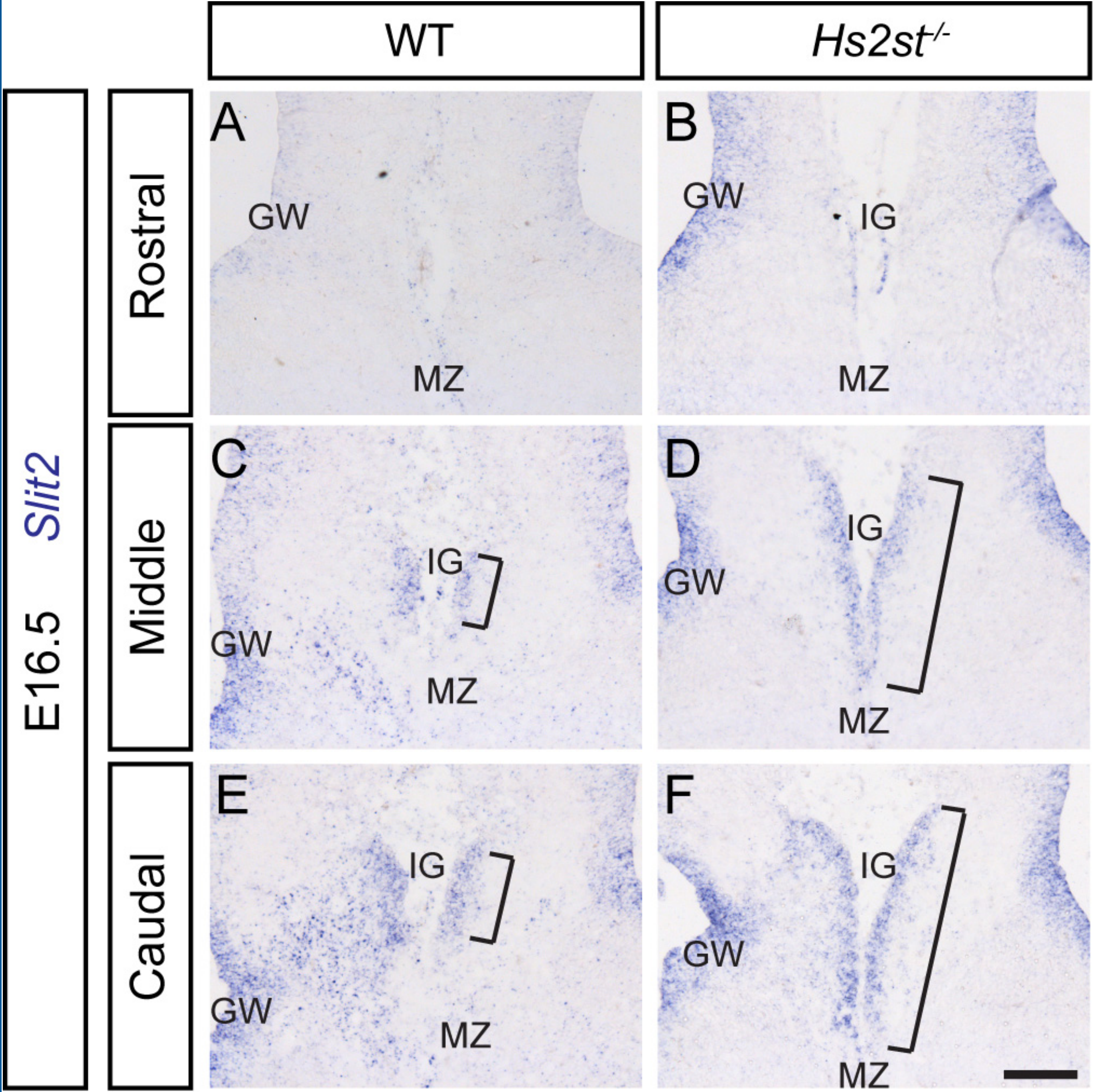

JNeurosci Accepted Manuscript

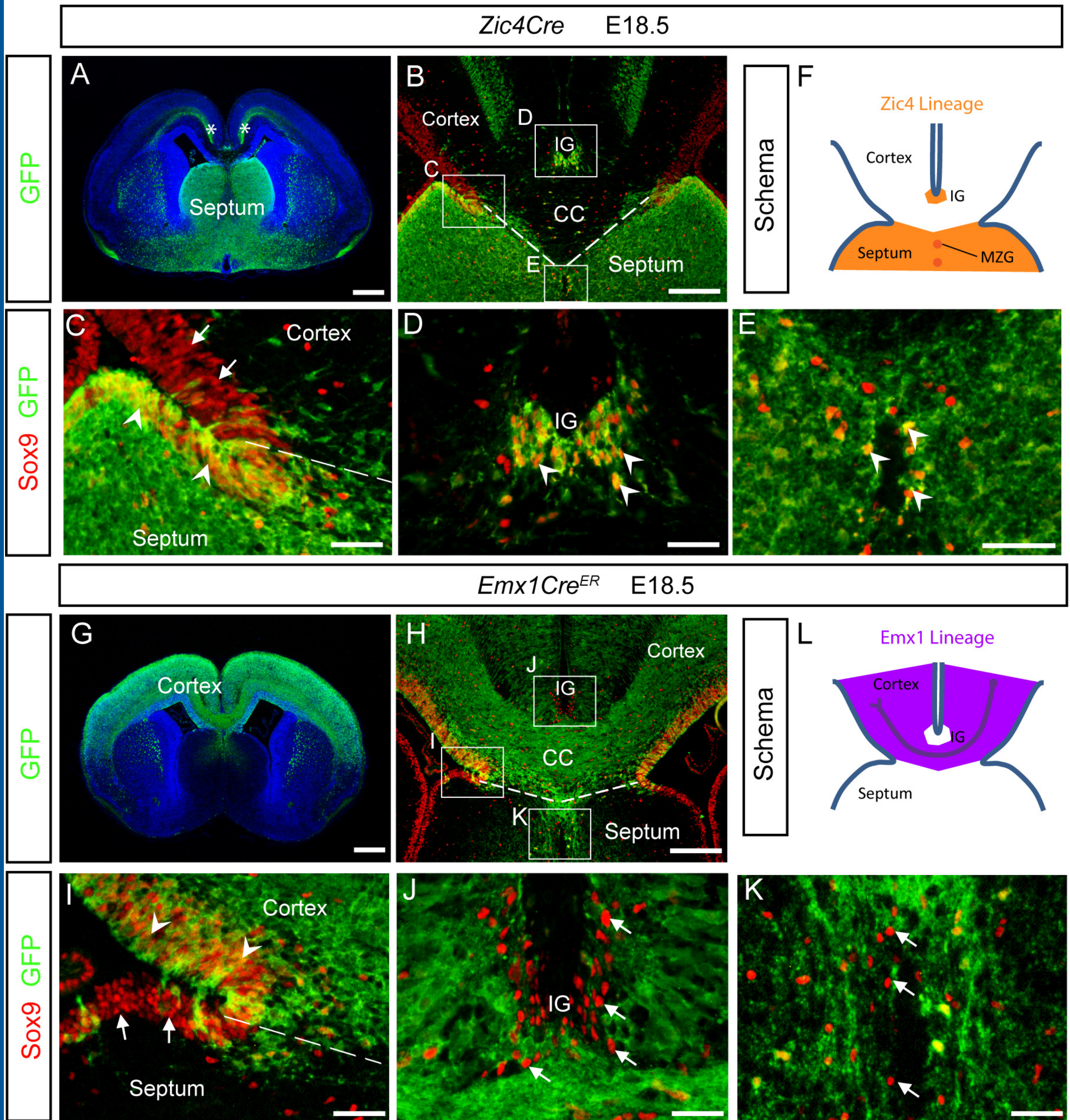

JNeurosci Accepted Manuscript

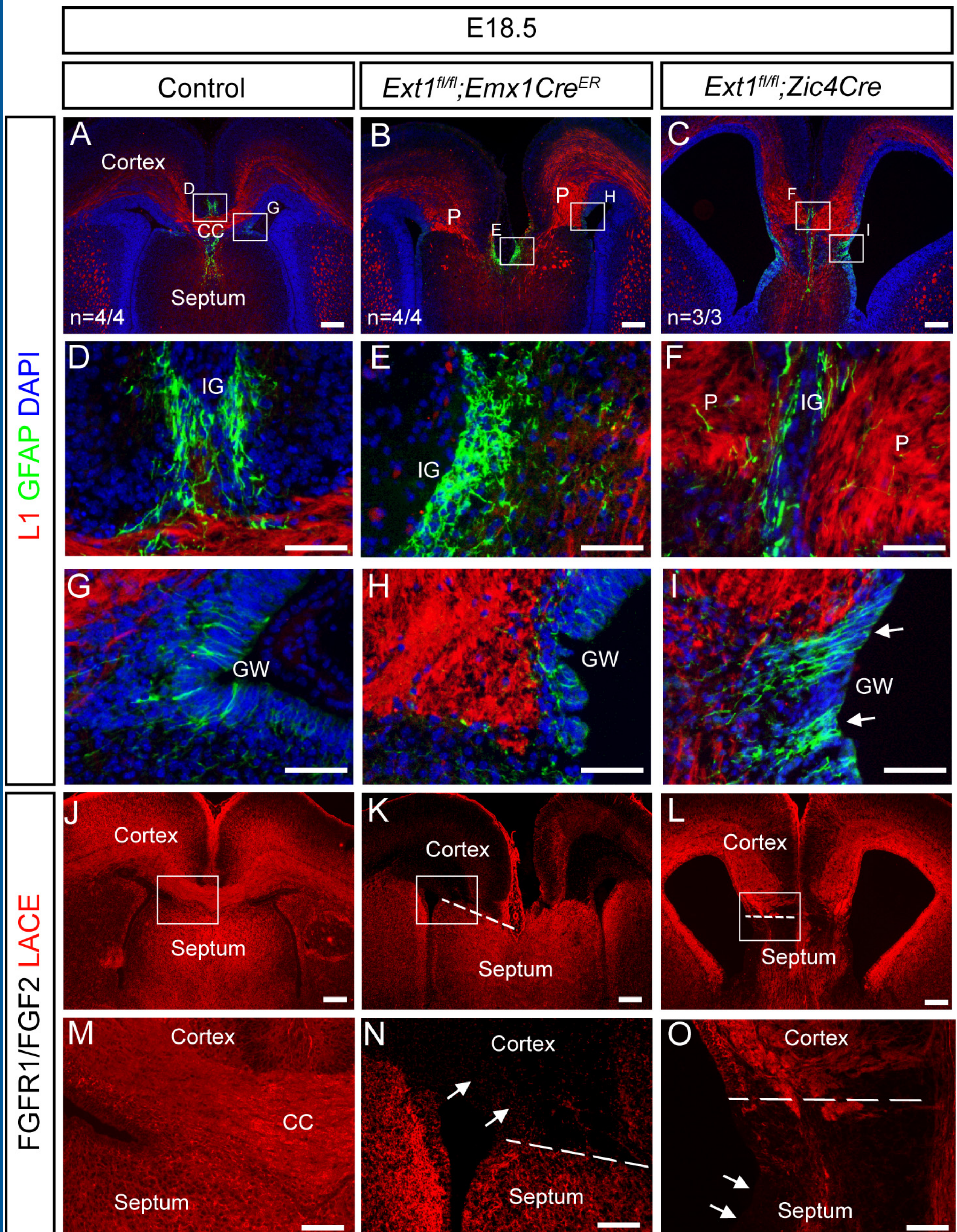

JNeurosci Accepted Manuscript

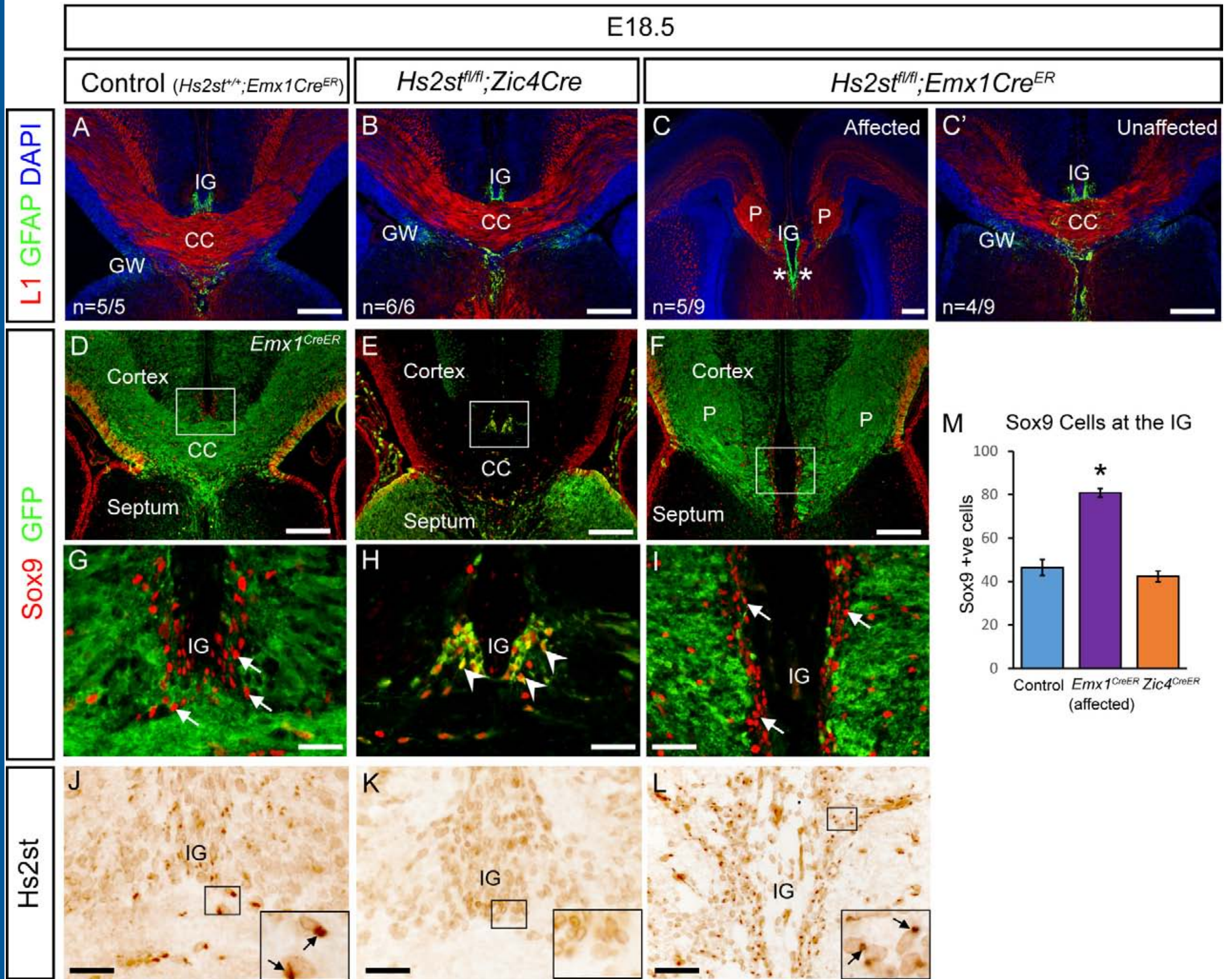

JNeurosci Accepted Manuscript

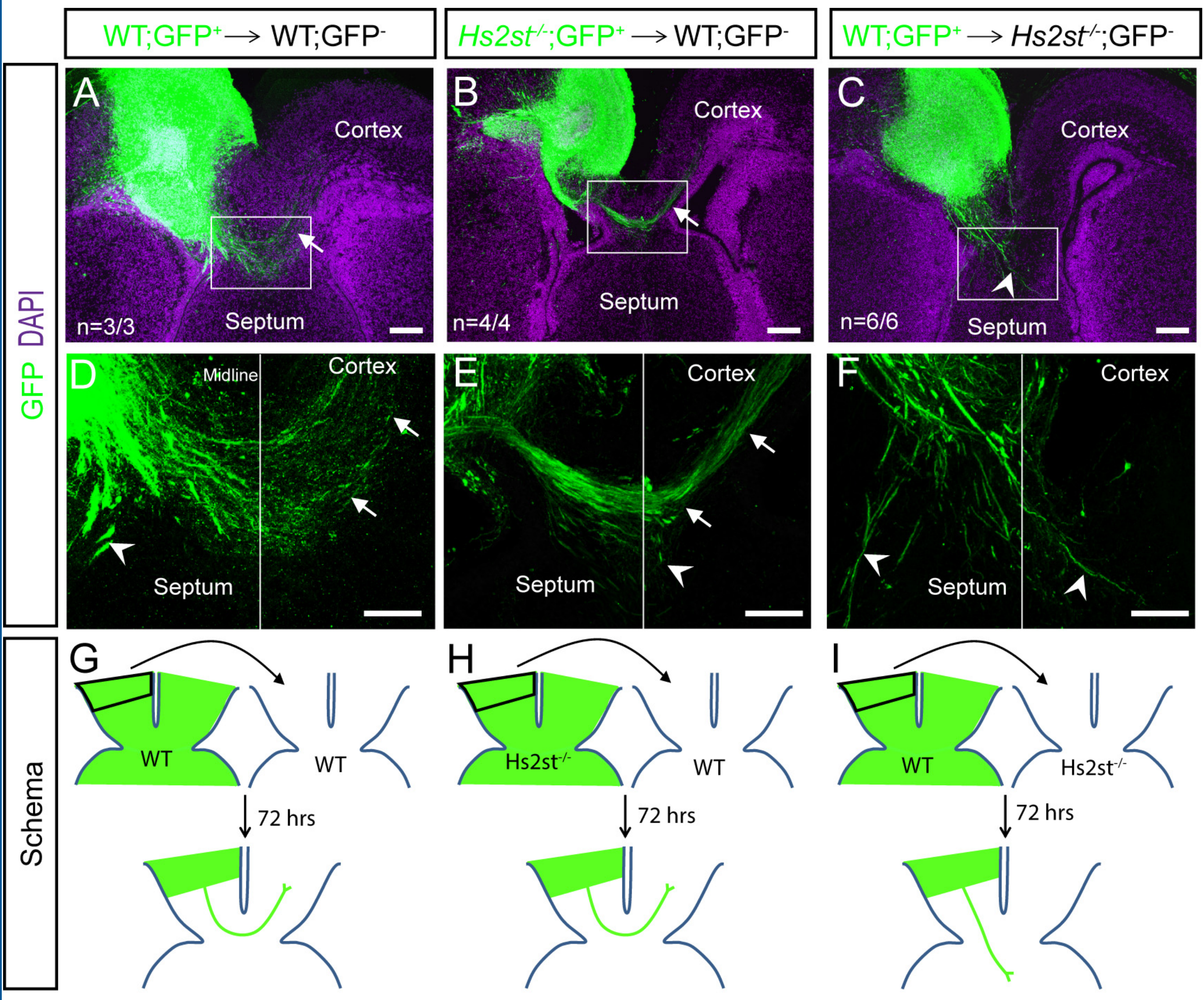

JNeurosci Accepted Manuscript

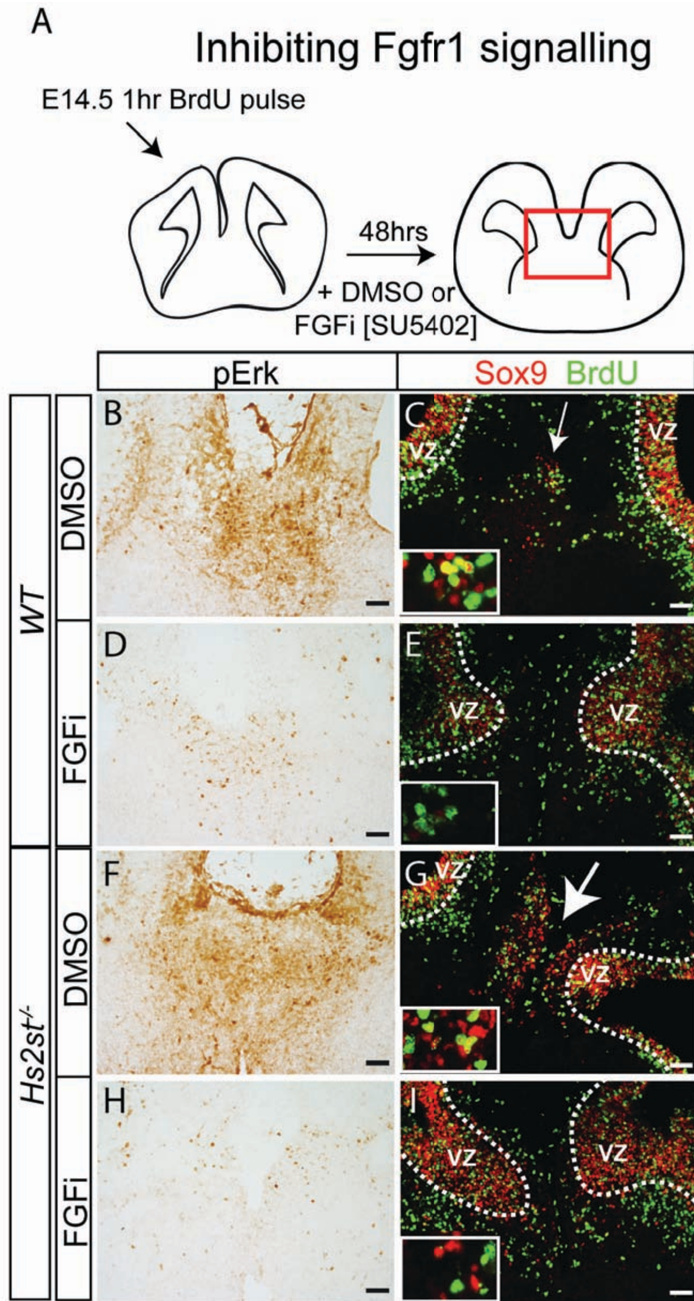

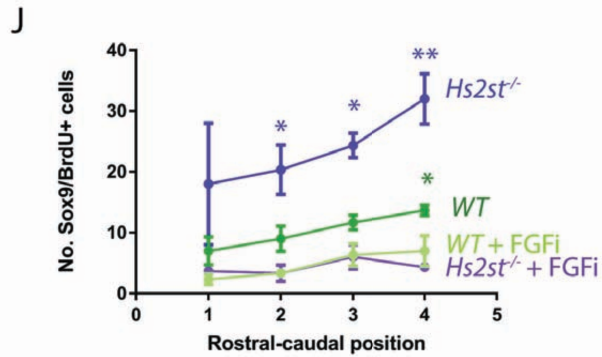

JNeurosci Accepted Manuscript

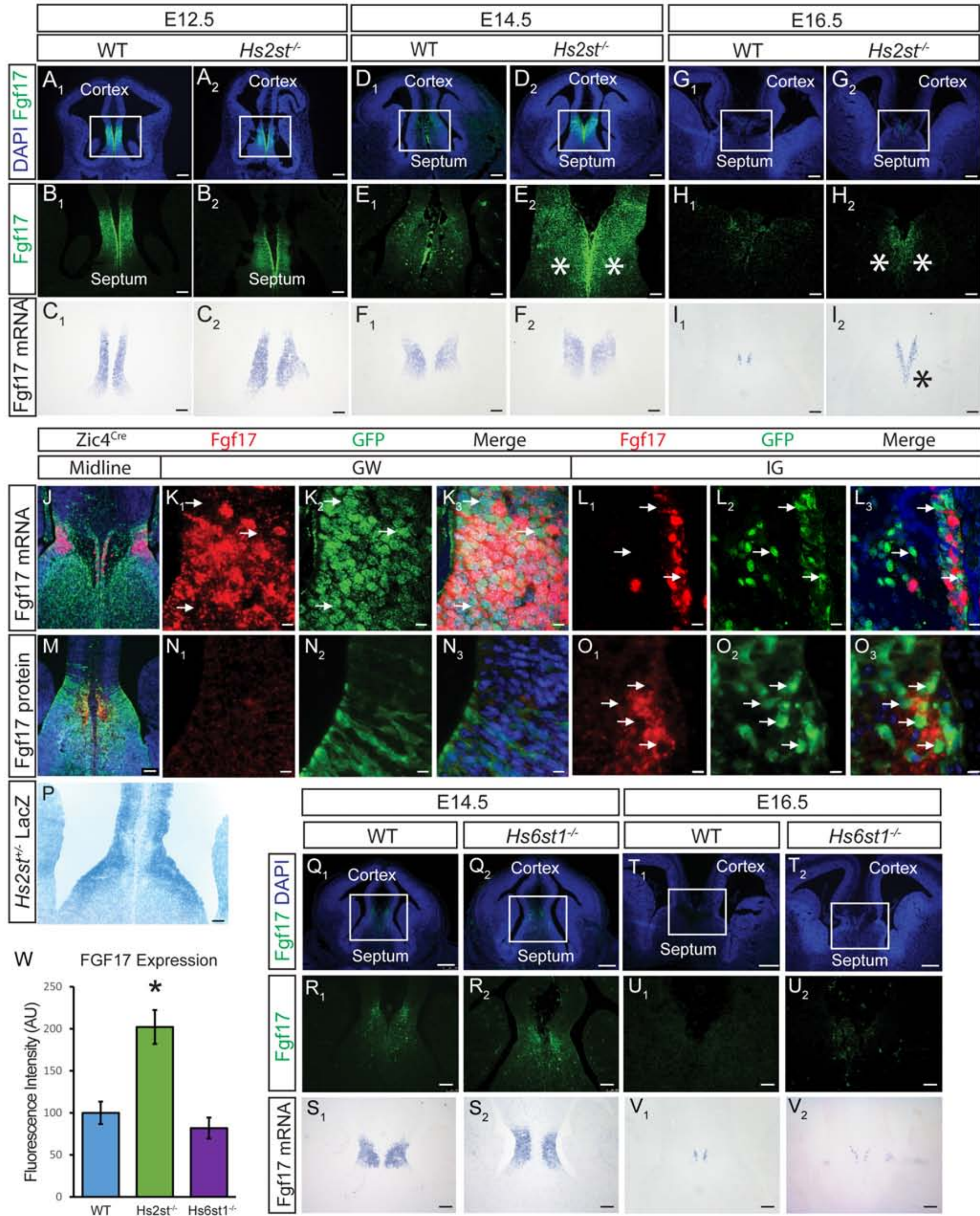

JNeurosci Accepted Manuscript

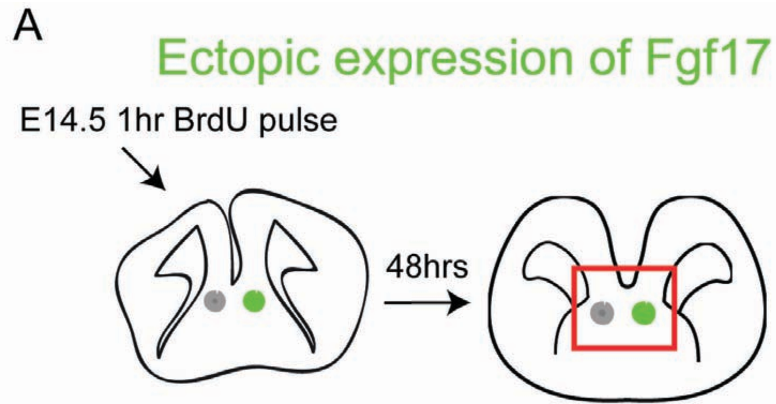

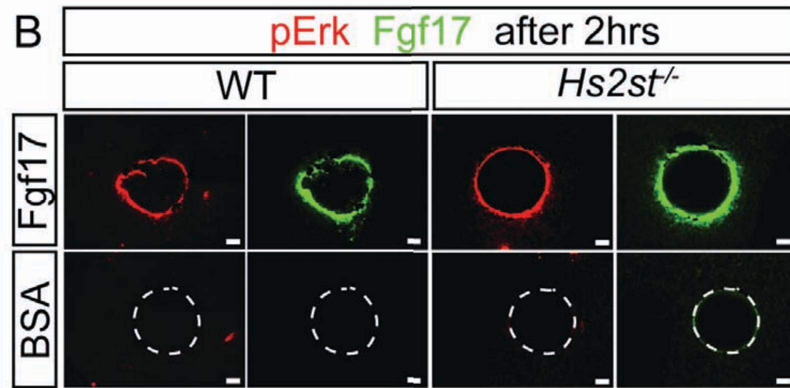

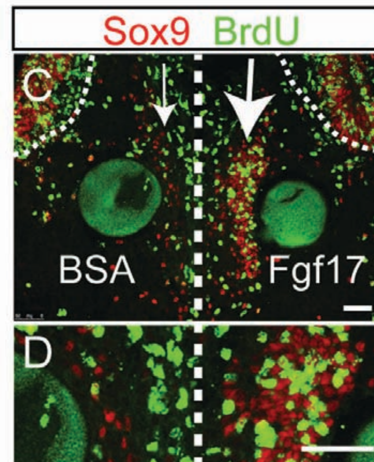

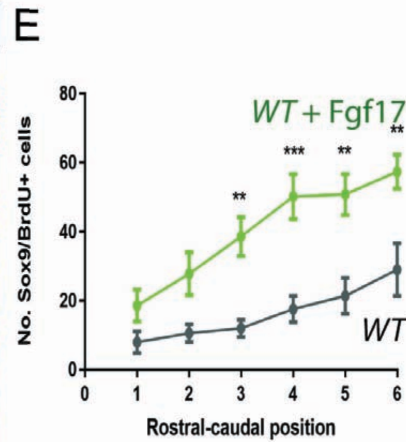

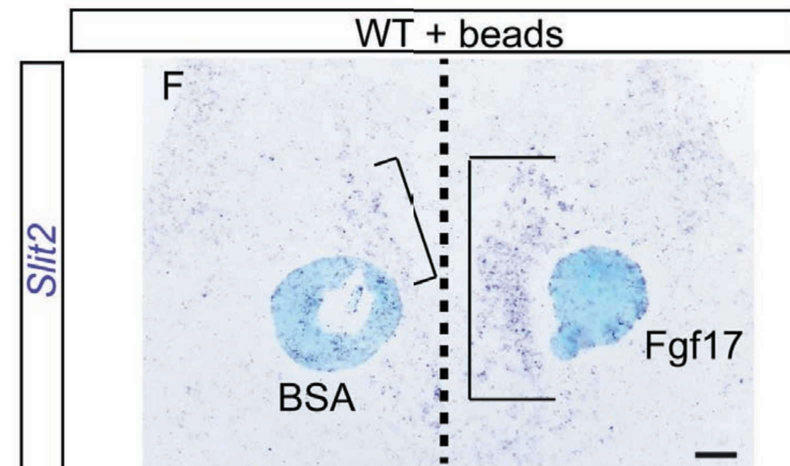

JNeurosci Accepted Manuscript

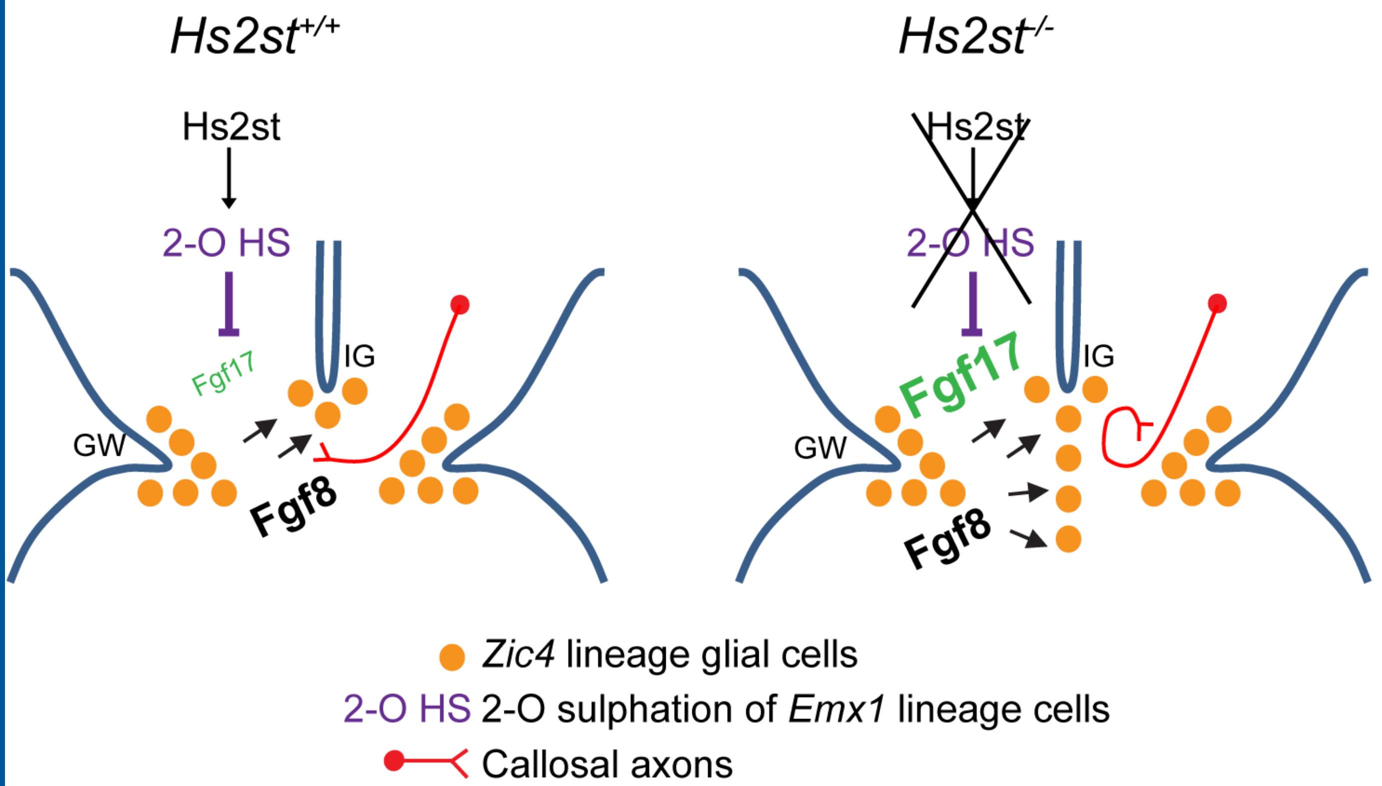

JNeurosci Accepted Manuscript